Engineering Structures 301 (2024) 117262

Contents lists available at ScienceDirect

Engineering Structures

journal homepage: www.elsevier.com/locate/engstruct

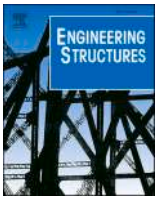

Experimental study of CRM-reinforced brick masonry panels: Cyclic shear-compression tests and compression tests

Carlo Vienni, Maurizio Orlando *, Luca Salvatori

University of Florence, Department of Civil and Environmental Engineering, Via di Santa Marta 3, Florence, Italy

ARTICLE INFO

Keywords:
Masonry
CRM
Structural strengthening
Shear-compression test
Compression test

ABSTRACT

The preservation of the building heritage is often accompanied by the necessity of ensuring adequate structural safety of existing buildings. Existing masonry structures are usually characterised by a high seismic vulnerability due to their low tensile strength; moreover, despite the significant compressive capacity, often masonry panels are not able to guarantee the safety level required by the current building codes under gravitational loads, due to their slenderness and the possible out-of-plane actions. In recent years, several systems have been developed for the reinforcement of masonry buildings based on the use of composite materials externally bonded to the structural elements. Among them, the CRM system can be used for the static and seismic reinforcement of masonry piers as an alternative to the traditional reinforced plaster. The CRM system consists of the application on the panel surfaces of a mortar layer about 3 cm thick reinforced with a glass fibre grid and connected to the wall through transversal connectors. Despite its increasing use, to date, few experimental and theoretical studies have been carried out focusing on the lateral behaviour of reinforced panels, especially regarding their flexural response and drift capacity, as well as a little number of studies are available regarding the contribution provided by CRM layers on the buckling failure of panels induced by vertical loads. This work presents an experimental campaign carried out at the Laboratory of Structures and Materials of the University of Florence. A series of tests for the mechanical characterisation of materials composing the masonry and the reinforcement has been at first performed; then, quasi-static cyclic shear-compression tests and compression tests on solid brick masonry panels strengthened with CRM have been performed, considering the application of the CRM on a single or both faces of the walls. Tests allowed the assessment of the mechanical properties of the retrofitting system and its adhesion to the substrate and highlighted the advantages and limitations produced in the structural response of reinforced walls, both for horizontal and vertical loading.

1. Introduction

The conservation of building heritage is one of the most important challenges in the construction field. The recent earthquakes in Italy have clearly shown the high seismic vulnerability of existing buildings, in particular of masonry structures characterised by poor-quality materials and poor connections between resisting elements. Several systems have been developed to improve masonry structures' mechanical characteristics and load-bearing capacity. In recent years, innovative composite systems externally bonded to masonry surfaces have been widely used [1,2]. Inorganic-matrix composites are increasingly used to reinforce existing buildings, thanks to the considerable advantages provided by the mortar coating, such as the reversibility of the intervention, the simplicity of application on irregular supports, the chemical compatibility with masonry substrate and the vapour permeability [3]. Three different types of inorganic matrix composites can be identified, depending on the typology of the reinforcement grid and the thickness of the matrix: Fibre Reinforced Cementitious Matrix (FRCM), Composite Reinforced Mortar (CRM) and Fibre Reinforced Concrete (FRC) systems. FRCM systems are composed of a thin layer of mortar, usually ranging between 10 and 20 mm, reinforced with a non-rigid textile; CRM, instead, is characterised by a thicker layer of mortar ranging from 30 to 50 mm reinforced with a rigid glass fibre grid; finally, FRC systems is a concrete coating containing short discrete fibres uniformly distributed and randomly oriented. Recently, several works have been carried out to study the effectiveness of these systems on different masonry members such as walls, arches, and columns. Tests on full-scale buildings are rare due to the onerous setup, although recently some experimental

* Corresponding author.
E-mail address: maurizio.orlando@unifi.it (M. Orlando).

https://doi.org/10.1016/j.engstruct.2023.117262
Received 19 July 2023; Received in revised form 22 October 2023; Accepted 26 November 2023
Available online 15 December 2023

campaigns have been conducted [4,5]. Despite that, regarding the effectiveness of CRM systems in increasing the seismic and load-bearing capacity of panels, a limited number of studies are still available in the scientific literature. A clear mechanical characterisation procedure for the definition of resistance parameters of the CRM components has not yet been proposed, although some available works have shown a rather different behaviour with respect to the response of FRCM systems due to the different geometric and mechanical characteristics of both the matrix and the grid [6,7]. The study of CRM-reinforced walls has been mostly carried out through diagonal compression tests [8–11] to define the increase in tensile strength [12]; however, these tests do not provide crucial information on the lateral behaviour of reinforced panels such as their flexural capacity and the influence of CRM application on the ultimate displacement. Cyclic shear-compression tests appear to be more suitable to study the seismic response of panels; in Boem, 2022 [13], a literature review of experimental and numerical studies focusing on masonry panels strengthened with FRCM and CRM systems was carried out showing the lack of experimental in-plane cyclic tests. For this reason, some studies have been carried out in the last years: in Gattesco et al., 2023 [14] in-plane cyclic tests were carried out on unreinforced and CRM-reinforced stone walls, evidencing the capability of the reinforcement in increasing both the shear strength and the displacement capacity. In [5] authors investigated the efficiency of CRM through a full-scale cyclic test on a two-storey building, evidencing the role of artificial diatones in preventing the leaves separation and mortar detachment and the importance of the connection between the coating and the foundation. Also, in Guerrini et al., 2023 [15] shear compression tests were performed on a CRM-reinforced stone masonry pier including portions of adjoining spandrels placed above and below to evaluate the effect of reinforced anchoring in the wall edges. Besides the seismic retrofitting, the reinforced plaster technique can also be applied to increase the load-bearing capacity of walls subject to gravitational loads: for this purpose, Italian Building Code NTC 2018 [16,17] provides some amplification coefficients of the masonry compressive strength to consider the contribution provided by the plaster application. These amplification coefficients are commonly applied to quantify the efficiency of CRM systems, despite in the current literature there are still few studies focusing on the compressive response of reinforced panels. Donnini et al., 2021 [18] performed uniaxial compression tests on brick and tuff panels, showing that the influence of the plaster can be rather limited in the case of mortar layers not directly loaded at the extremities (a common situation in case of discontinuity of the reinforcement at the floor's level). In Pinho et al., 2012 [19], uniaxial compression tests were carried out on irregular rubble stone masonry walls strengthened with two concrete layers 50 mm thick reinforced with a steel mesh considering two different setups: concrete layers applied with transversal connectors through the thickness of the panels but not in contact with the foundation of the loading system or concrete layers in contact with the base but without transversal connectors. The authors showed that the presence of the plaster increased the compressive strength and the ductility of the panels with respect to unreinforced samples even in the case of centred load and disconnection at the base thanks to the confinement effect offered by the plaster layers and connectors reducing the disaggregation of the masonry; furthermore, the importance of providing the connection of the plaster in the foundation was shown, observing a significantly higher contribution of the reinforcement in case of contact with the base of the loading system. Bernat et al., 2013 [20] studied the contribution of an FRCM system against out-of-plane deflections in compressed masonry walls. Uniaxial compression tests were carried out on pinned-pinned restrained walls with a prescribed load eccentricity with or without reinforcement applied on the tensile side. Two different failure modes were observed: the URM walls failed by out-of-plane buckling due to the tensile fracture of a bed joint while the TRM strengthened walls failed by compression near their upper or lower edge, showing an increase of about 2 times the ultimate compressive strength. Literature results suggest that the effect of reinforcement for vertical loads, in the case of coating not effectively anchored at the ends, is to increase the strength of the panel thanks to the inhibition of out-of-plane lateral buckling. In this work, the behaviour of strengthened panels under horizontal and vertical actions was investigated by performing an experimental campaign consisting of quasi-static cyclic shear-compression tests and compression tests on solid brick masonry panels reinforced with a CRM system commercially available. Firstly, a series of mechanical characterisation tests have been performed on masonry walls and CRM components. Then six shear-compression tests and three compression tests were carried out to evaluate the efficiency of the strengthening technique. This work complements the preliminary results published in Vienni et al., 2023 [21,22].

2. Characterisation tests of materials

2.1. Masonry

Masonry employed in the work was built using solid clay bricks with dimensions 230 × 115 × 55 mm^3. The compressive strength in the vertical direction of the units was determined by direct compression tests on five single bricks, performed according to EN 772–1 [23]. The average value of brick compressive strength was equal to $f_b = 37.01$ MPa (CoV = 3.2%). The mortar was composed of a mixture of cement Portland, lime and sand and was classified by the manufacturer as a mortar M2.5 according to EN 1015–11 [24]. Its characterisation was carried out through compression and bending tests on prisms with size 160 × 40 × 40 mm^3. For each set of tests carried out, six prisms have been tested: wallets used for the characterisation of compressive strength of the masonry and for bond tests were made up of a mortar characterised by $f_{c,mortar}$= 5.11 MPa (CoV = 4.5%), samples used for concentric and eccentric compression tests by joints with resistance $f_{c,mortar} = 4.27$ MPa (CoV = 6.0%), and finally, walls used in shear-compression tests by a mortar with $f_{c,mortar} = 4.15$ MPa (CoV = 2.0%). These differences in mortar strength can be attributed to the high variability of the several parameters involved, such as the environmental conditions at the time of casting, the number of beats for the constipation of the prisms and the removal of air, the amount of water used in the preparation of the specimens. A total of eighteen bending/compression tests have been performed, obtaining an average value of compressive and flexural strength of the mortar $f_{c,mortar} = 4.60$ MPa (CoV=10.5%) and $f_{f,mortar} = 1.60$ MPa (CoV=15.7%), respectively. To evaluate the compressive strength and elastic modulus of the masonry three small wallets with dimensions 230 × 115 × 400 mm^3 were built. Compression tests were carried out according to the EN 1052–1 testing protocol [25]. The average compressive strength and the elastic modulus of the masonry were $f_{c,m} = 14.40$ MPa (CoV=3.7%) and $E_m = 4848$ MPa (CoV=12.7%), respectively.

2.2. Mortar of the CRM system

Bending and compressive tests have been carried out to define the flexural and compressive strength of the mortar composing the matrix of the CRM system. The mortar used was a commercially available coating for the realisation of CRM systems composed of pure hydraulic lime mortar NHL 3.5; according to the manufacturer's datasheet, it was classified as M15 mortar (EN 1015–11) with an elastic modulus $E_{pl} \geq$ 8500 MPa. The thickness of the layers applied on masonry supports was 30 mm. The average compressive strength was found $f_{c,pl} = 13.80$ MPa (CoV = 8.3%), and the average value of flexural strength was $f_{f,pl} = 4.78$ MPa (CoV = 7.0%). The Young modulus was indirectly derived from the results of clamping-grip tests and was equal to about $E_{pl} = 10$ GPa. The procedure to estimate E_{pl} will be described in the following Section focusing on tensile tests on CRM coupons.

2.3. Tensile tests on bare yarns

The grid constituting the reinforcement of the mortar matrix was composed of yarns arranged in weft (x-axis) and warp (y-axis) directions. The yarns were composed of glass fibres impregnated with epoxy resin. Yarns in the weft direction consisted of an FRP single wire, while in the orthogonal direction of two twisted sub-yarns. The grid had a square mesh with a size 80 × 80 mm^2. The weight of the grid was 490 g/m^2. The dimensions of the yarns were obtained according to the manufacturer's data sheet [26]. The mechanical properties of the yarns are provided in Table 1, where A_y indicates the overall cross-section of a single yarn including the fibres and the resin, A_{fib} indicates the actual area of the fibres inside the yarn and φ is the equivalent diameter of the twisted yarns. The mechanical properties of the grid have been investigated through tensile tests on single yarns, in the weft (n° 5 specimens) and warp (n° 5 specimens) direction. The length of the yarns was equal to L_{yarn} = 560 mm and they were instrumented with a displacement transducer with a gauge length equal to 240 mm. Tests were conducted by applying the load to the ends of the wires in displacement control with a rate of 0.008 mm/s. To avoid damage at the yarn ends, specimens were equipped with end grips composed of aluminium cylinders filled with epoxy resin; the length of the anchorages was chosen to avoid sliding between the fibres and the clamp and was set 80 mm. The cross-section used to define stress and strain was the nominal area of a single yarn, A_y, according to Italian Guidelines recently released for CRM systems [27]. The tensile rupture occurs by spalling of the glass fibres inside the resin in the X direction, while a sharper rupture was observed in the Y direction. A linear elastic behaviour until rupture was obtained. Tensile strength, elastic modulus, and strain at rupture equal to $\sigma_{f,x}$ = 1081 MPa, $\sigma_{f,y}$ = 641 MPa, $E_{f,x}$ = 57 GPa, $E_{f,y}$ = 35 GPa and $\varepsilon_{f,x}$ = 1.90%, $\varepsilon_{f,y}$ = 1.84% were obtained. The ultimate tensile load was higher in the X direction with respect to twisted yarns due to the higher fibre content inside a single wire ($A_{fib,x} > A_{fib,y}$).

2.4. Tensile tests on CRM coupons

The tensile behaviour of CRM systems, including the inorganic matrix and the grid, was studied through direct tensile tests. Two different setups can be used to perform tensile tests on composite coupons according to the end grips, namely clevis-grip and clamping-grip tests. Italian acceptance criteria for FRCM systems [28] recommend the use of the second approach, while the American guidelines [29] recommend the first to reproduce field boundary conditions from typical installation. Since in this work also bond tests have been performed, the clamping-grip setup was used. Two series of 5 specimens were prepared, considering in one case weft and in the other warp direction as longitudinal yarns (i.e., parallel to tensile load direction). Rectangular coupons with dimensions of 640 × 120 × 30 mm^3 reinforced using two longitudinal yarns and eight transversal yarns were fabricated. Samples were cured at laboratory conditions for about 90 days before testing. Coupon ends were clamped using two steel plates 10 mm thick for each side; the plates were gripped together using six bolts 10 mm in diameter, which allowed the application of the compressive action on the ends of the coupon necessary to avoid sliding between the mortar and the plates. Two anchorage lengths were considered, namely 120 mm for three specimens and 160 mm for the remaining 7 specimens, to evaluate the anchorage influence on the tensile response. A designed compression load of 90 kN was applied by checking the preload of the bolts using a torque wrench. The compressive load, distributed on an area of 160 × 120 mm^2 or 120 × 120 mm^2 (anchorage surfaces of coupons) produced compression stress of about 4.68 or 6.25 MPa, respectively, in any case lower than the mortar compressive strength. Specimens were equipped with neoprene sheets glued to the coupon ends to avoid local damage and to ensure a uniform distribution of the compressive action on the bonded area. The tensile load was applied by pulling the steel plates. Tests were carried out in displacement control by monotonically increasing the vertical displacement at a rate of 0.0083 mm/s. Two extensometers with a gauge length of 260 mm were applied to the central portion of the specimens to measure the axial strain. Specimens were named according to the notation *TC_L_O_n_cr*, where *-TC* indicates Tensile Coupon, *-L* the length of the clamped area, *-O* the longitudinal orientation of the fibres (namely *X* for weft or *Y* for warp direction), *-n* the specimen progressive number (from 1 to 5), *-cr* indicates possible cracks in the matrix before testing. The obtained stress-strain curves are plotted in Figs. 1a and 1b for the weft and warp direction, respectively. The stresses were calculated by dividing the tensile load by the cross-section area of the two longitudinal yarns (2•$A_{y,x}$ = 2•9.90; 2•$A_{y,y}$ = 2•11.90). Table 2 summarises the main results: F_{cr} is the load registered at the formation of the first crack in the mortar, σ_{cr} is the tensile stress on the mortar calculated by dividing F_{cr} by the plaster cross-section (120 × 30 mm^2), F_u and σ_u are the ultimate load and the ultimate stress before rupture, E_1 and E_2 are the slopes of the first (uncracked stage) and the second (cracked stage) branches of the curves. The typical trilinear behaviour characterising reinforced mortar coupons [30] was obtained. A first elastic branch was observed until the formation of the first cracks in the mortar. Cracks orthogonal to tensile load occurred, aligned with transversal yarns; matrix cracking was induced by the reduction of the matrix cross-sectional area in the cross-sections corresponding to the grid intersections.

The cracks opened progressively: first horizontal cracks were observed in the middle height of the specimens (Fig. 2a), and then further cracks opened both centrally and at the clamped ends. During the crack formation, sudden decreases in the applied load were registered. As the number of cracks stabilised, the second branch started: in this second phase the load increased linearly with a slope close to the one of dry fibres until failure. Since the cracks opened inside the anchor length, the gradual extraction of the longitudinal FRP yarns from the clamped ends emerged and induced the failure due to slippage at the matrix-to-mesh interface (Fig. 2b). The tensile failure of GFRP yarns was never reached.

To assess the relevance of transversal yarns included inside the bonded area, three samples *TC_120_X_05, TC_120_Y_04* and *TC_120_Y_05* were tested with a reduced anchor length of 120 mm, including only one transversal yarn in the clamps. For these tests, as expected, a lower ultimate load was obtained due to the premature slippage of the fibres; similar results were obtained by Gattesco et al., 2017 [7]. In Table 2 the results of specimens with a reduced anchor length are shown in red and are not used to calculate the average properties and the coefficients of variation. The cracked branches of the trilinear curves remained almost parallel to the stiffness of the dry fibres until failure, demonstrating that the occurrence of matrix cracks outside the extensometer gauge length did not strongly affect the deformability measure. Due to the slippage of the yarns inside the matrix, the average tensile strength of CRM coupons $\sigma_{u,x}$ = 503 MPa and $\sigma_{u,y}$ = 485 MPa were significantly lower than the one of bare yarns. The ultimate loads obtained with longitudinal yarns in the weft or the warp directions were quite similar, showing the limited influence of the yarn's direction in the mortar-fibre interface strength. From clamping grip tests, also some information about the mechanical properties of the mortar composing the CRM system has been obtained. Firstly, the tensile strength of the mortar was evaluated by dividing the load acting at the formation of the first crack by the cross-section of the

Table 1
Geometrical properties of the GFRP grid according to the manufacturer's technical sheet.

	Mesh pitch [mm^2]	Nominal dimensions of the yarns [mm]	Nominal area A_y [mm^2]	Fibre area A_{fib} [mm^2]
Single yarn (x)	80 × 80	5.5 × 1.8	9.9	7.2
Twisted yarn (y)		φ 3.9	11.9	5.7

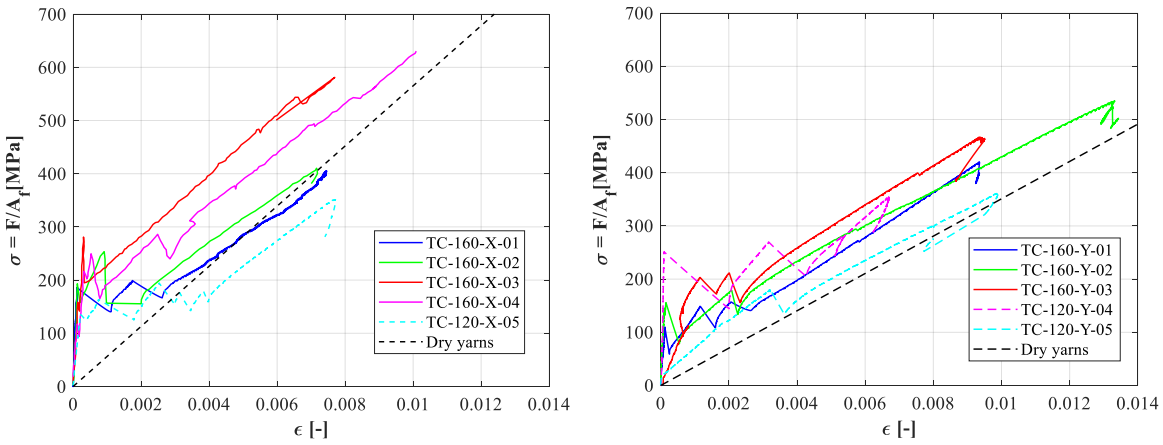

Fig. 1. Trilinear behaviour of CRM coupons: (a) longitudinal yarns in the weft direction; (b) longitudinal yarns in the warp direction.

Table 2
Results of clamping grip tests on CRM coupons.

	F_{cr} [kN]	$\sigma_{cr} = F_{cr}/A_{pl}$ [MPa]	F_u [kN]	$\sigma_u = F_u/A_y$ [MPa]	E_1 [Gpa]	E_2 [Gpa]
TC_160_X_01	3.67	1.02	8.0	406	1712	46
TC_160_X_02	3.81	1.06	8.2	414	-	46
TC_160_X_03	3.06	0.85	11.5	581	1631	55
TC_160_X_04	2.49	0.69	12.1	612	-	50
TC_120_X_05	3.20	0.88	6.9	351	-	49
Average	**3.26**	**0.91**	**10.0**	**503**	**1671**	**49**
CoV (%)		16%		19%	2%	7%
	F_{cr} [kN]	$\sigma_{cr} = F_{cr}/A_{pl}$ [MPa]	F_u [kN]	$\sigma_u = F_u/A_y$ [MPa]	E_1 [Gpa]	E_2 [Gpa]
TC_160_Y_01	2.62	0.73	10.8	454	1407	39
TC_160_Y_02	3.71	1.03	12.7	535	1552	33
TC_160_Y_03_cr	-	-	11.1	467	-	40
TC_120_Y_04	5.88	1.66	8.4	354	-	41
TC_120_Y_05_cr	-	-	8.6	363	-	34
Average	**3.16**	**0.88**	**11.5**	**485**	**1479**	**37**
CoV (%)		17%		7%	5%	9%

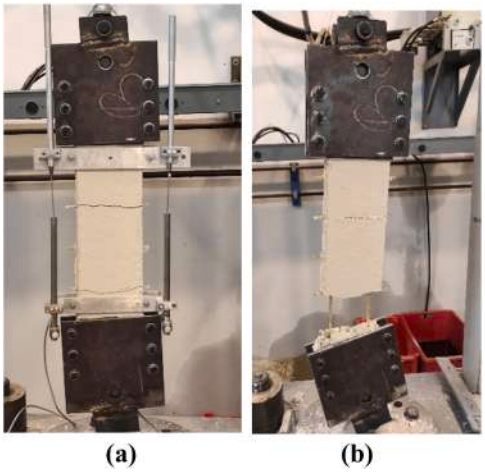

Fig. 2. Failure mechanism of coupons: (a) initial cracking in the central part of the specimen aligned with transversal yarns; (b) failure due to slippage of the yarns inside the matrix.

plaster: the obtained tensile strength was equal to $f_{t,pl} = 0.90$ MPa (average value between all 160 mm anchored tests in Table 2). This value can be compared with the tensile strength obtained using the formulation proposed by Model Code [31] for the assessment of the concrete tensile strength from its flexural strength $f_{t,pl} = \frac{f_{f,pl} \bullet 0.06 \bullet h_b^{0.7}}{1+0.06 \bullet h_b^{0.7}}$, where h_b is the depth of the beam used in the bending test (in this case 40 mm) and $f_{f,pl} = 4.35$ MPa the flexural strength of the mortar obtained from the bending test for the set used to realise CRM coupon. According to [29] the mortar tensile strength is equal to $f_{t,pl\_MC} = 1.90$ MPa, about two times higher than the one obtained using the load corresponding to the first cracking. The reduced value of the tensile strength corresponding to the occurrence of the first cracks in the coupon may probably have been caused by the stress concentrations at the warp-to-weft joints, which caused a stress distribution not uniformly applied on the whole cross-section of the plaster. However, it should be noted that the stabilisation of the cracking phase occurred in the tensile load range of 2.50–5.40 kN: if the higher value, namely the load corresponding to the opening of the last crack before stabilisation, was used, a value of tensile strength of the mortar of about 1.50 MPa would be obtained, which would be more similar to that evaluated by the procedure proposed by the Model Code, and about ten times lower than the compressive strength of the plaster. In addition to the tensile strength, the elastic modulus of the mortar can also be estimated from the coupon tests: once the slope of the first branch was known, the elastic modulus of the mortar was calculated assuming that in the initial phase both the mortar and the fibres were characterised by a linear elastic behaviour and assuming a perfect adhesion between fibres and mortar. By equalising axial strains in the fibres and mortar it was possible to obtain an elastic modulus of the plaster equal to $E_{pl} = 9520$ MPa, which was in good agreement with the one provided by the manufacturer's technical sheet (i.e., $E_{pl} \geq 8500$ MPa).

2.5. Bond tests

The effectiveness of externally bonded reinforcement is strongly related to the adhesion between different components, namely masonry-to-matrix and matrix-to-grid interfaces [1,2]. In this work, 12 single-lap shear bond tests have been carried out to evaluate the CRM-to-brick masonry interface behaviour. Twelve solid clay bricks wallets with dimensions of 230 × 120 x 390 mm^3 were built and cured at laboratory conditions for 60 days before the application of CRM. Then, CRM strips were applied to the support considering two different layouts: the first six specimens were tested considering a bonded length equal to 300 mm; the second six specimens were tested considering an anchor length of 300 mm and the presence of one steel connector applied at the middle-height of the bonded length. For each set, three samples were tested considering longitudinal yarns in the weft direction and three with longitudinal yarns in the warp direction. The walls were only cleaned and wet before the application of the plaster. CRM

reinforcement had a thickness of 30 mm and comprised two longitudinal yarns. Once the CRM was applied, specimens were cured at laboratory conditions for 30 days before testing. The upper portion of the grid was left unbonded for a length of 320 mm to ensure the application of the tensile load. A push-pull test was carried out: masonry walls were restrained against vertical movements with a steel plate connected to the base of the test bench through four steel bars; the upper ends of the fibres were clamped to the testing machine for a length of 70 mm using two steel tabs glued to the yarns to avoid damage on the load application area and to ensure the load transfer between the clamp and the yarns. Tests were carried out in displacement control at a constant rate of 0.0033 mm/s. Four LVDTs were used to measure the displacements of the fibres and the matrix. Axial displacements of the fabric just outside of the bonded length were measured, *s1* and *s2*; axial displacements of the upper portion of the mortar were measured by glueing L-shaped profiles to the plaster just below the loaded end using two further LVDTs, *s3* and *s4*. The two pairs of LVDTs were placed one on the right and one on the left side of the specimens to evaluate any asymmetries in the response. The displacement of the yarns with respect to the wall s_f was the average between *s1* and *s2*; the displacement of the upper portion of the mortar s_{pl} was the average between *s3* and *s4*. The sliding of the fibre inside the upper portion of the matrix can be calculated as $sld = s_f - s_{pl}$. A sketch of the test setup is provided in Fig. 3. Specimens were named according to the notation *BT_L_O_n_C*, where *-BT* indicates Bond Test, *-L* the bonded length of plaster (namely, 300 mm), *-O* the longitudinal orientation of the fibres (namely *X* for weft or *Y* for warp direction), *-n* the specimen progressive number (from 1 to 3), *-C* indicates the possible presence of the helical steel connector. Results are provided in Table 3 in terms of observed failure mechanisms, peak load before rupture F_{deb}, ultimate stress in the fabric before rupture σ_{deb} calculated as the ratio between F_{deb} and the nominal area of the yarns A_y, shear strength of the interface τ_u calculated as the ratio between the peak load and the total area of the bonded surface A_b (i.e., 300 ×120 mm^2). Regarding the failure mechanism, the notation provided in the Italian guideline CNR DT 215/2018 was used, namely, B indicates debonding at the masonry-to-mortar interface, E slippage of the fibres and matrix cracking, F tensile rupture of the yarns.

The results of the first set of tests showed values quite close to each other, regardless of the longitudinal direction of the yarns: the orientation of the yarns, indeed, was expected to have a limited influence on the bond results since even in the tensile tests on CRM coupons a similar behaviour of weft and warp yarns-to-matrix interface was observed. A greater difference between the two directions has been observed for the second set; however, these differences can be attributed to the greater uncertainties characterising these samples, such as the actual amount of penetrated plaster behind the connectors. The results in terms of applied tensile load *F* to yarns' slip s_f are provided in Fig. 4.

BT_300_X_3_C was plotted in red colour in Table 3 and with dot lines in Fig. 5 because it was characterised by a significant misalignment of the yarns inside the matrix which provided lower values of the ultimate load; the results of this test were not considered in the calculation of average values of mechanical parameters. All six specimens of the 1st set showed the same failure mechanism, due to the debonding at the matrix-to-masonry interface without significant damage in the support, usually preceded by the cracking of the upper portion of the mortar (E + B), as shown in Fig. 5. The mean value of the peak load was equal to 8.53 kN and the average shear resistance of the interface to $\tau_u = 0.24$ MPa. The cracks formed at the same height as the mesh grid intersections evidencing the role of the transversal yarns in the transfer of the tensile load to the matrix (Fig. 5f).

To evaluate the influence of the connectors on the load transfer at the masonry-mortar interface, six specimens were built by inserting a connector in the middle of the adhesion length (2nd set). It is worth noting that the presence of the connector in this type of test is not representative of the overall response of a reinforced wall, since 4–5 connectors/m^2 are usually placed in a real scenario (1 connector/0.2 m^2) while in this case the influence of the connector was studied on an area of about 0.036 m^2. The connections were given by helical inox steel bars characterised by yielding stress $f_y > 190$ MPa (type AISI 304), extraction strength equal to 1.11 kN considering an anchor length of 280 mm, nominal diameter equal to 10 mm (all the properties were obtained from the manufacturer's datasheet). Connectors were applied dry, making a pre-hole of 8 mm diameter and 200 mm length; the connector was then inserted with a dowel hammer for 200 mm and bent above the grid for 10 mm. Five of the six specimens of the 2nd set showed a failure mechanism due to detachment at the matrix-to-masonry interface, more evident in the lower portion of the CRM strip, usually preceded by the cracking of the upper portion of the mortar (E + B). Only the specimen *BT_300_Y_2_C* was characterised by a different failure mechanism due to the tensile rupture of a single wire. This rupture, premature if compared to the others (6.16 kN), was probably caused by an asymmetry in the application of the load through the machine grip. The mean value of the peak load was equal to 9.02 kN and the average shear resistance of the interface to 0.25 MPa. The average ultimate load is about 5.5% greater than the one obtained in the first set of tests (same anchor length but without connectors), which indicates that the ultimate load was not strongly affected by the connector and the load-transfer mechanism at the matrix-to-masonry interface was mainly related to the adhesion between the two components; once the adhesion between mortar and support failed, the connector allowed the CRM strip to remain attached to the wall but without a significant additional strength reserve. The ratio between the peak tensile load and the cross-section of the yarns gives the value of tensile stress in the grid at the time of detachment, corresponding to the

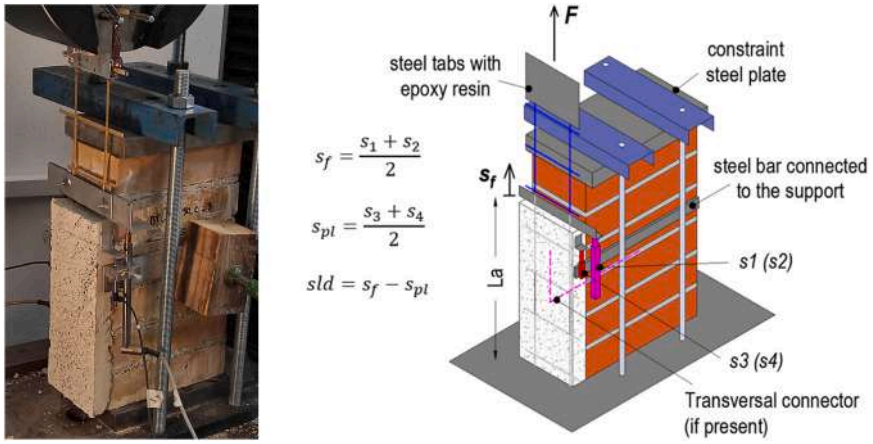

Fig. 3. Bond test setup and indications of the monitored quantities.

Table 3
Shear bond test results. First set of specimens with anchor length equal to 300 mm (longitudinal yarns in X or Y direction); second set with anchor length equal to 300 mm and connectors placed in the middle of the bonded length. The results of the specimen red-coloured were neglected due to fibre misalignment.

1st set - Weft	FM	F_{deb} [kN]	σ_{deb} [MPa]	τ_u [MPa]	1st set - Warp	FM	F_{deb} [kN]	σ_{deb} [MPa]	τ_u [MPa]
BT_300_X_1	E + B	7.68	388	0.21	*BT_300_Y_1*	E + B	10.25	430	0.28
BT_300_X_2	E + B	9.57	483	0.27	*BT_300_Y_2*	E + B	7.33	308	0.20
BT_300_X_3	E + B	7.51	379	0.21	*BT_300_Y_3*	E + B	8.83	371	0.25
	Average	**8.26**	**417**	**0.23**		**Average**	**8.80**	**370**	**0.24**
	CoV (%)		11.3%		Cov (%)		13.5%		
2nd set - Weft					2nd set - Warp				
BT_300_X_1_C	E + B	10.66	538	0.30	*BT_300_Y_1_C*	E + B	7.73	325	0.21
BT_300_X_2_C	E + B	11.15	563	0.31	*BT_300_Y_2_C*	F	6.16	259	0.17
BT_300_X_3_C	B	5.32	269	0.15	*BT_300_Y_3_C*	E + B	9.39	395	0.26
	Average	**10.90**	**550**	**0.30**		**Average**	**7.76**	**326**	**0.22**
	CoV (%)		24.2%		Cov (%)		17.0%		

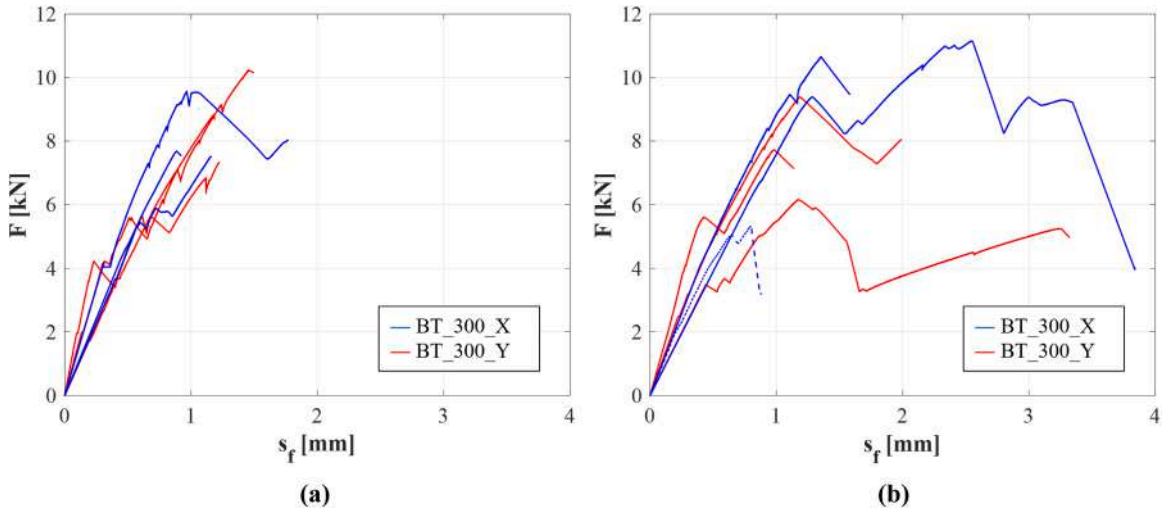

Fig. 4. Tensile load-fibre slip s_f responses obtained from bond tests. (a) 1st set: anchor length 300 mm; (b) 2nd set: anchor length 300 mm and connector applied at the centre of the bonded length.

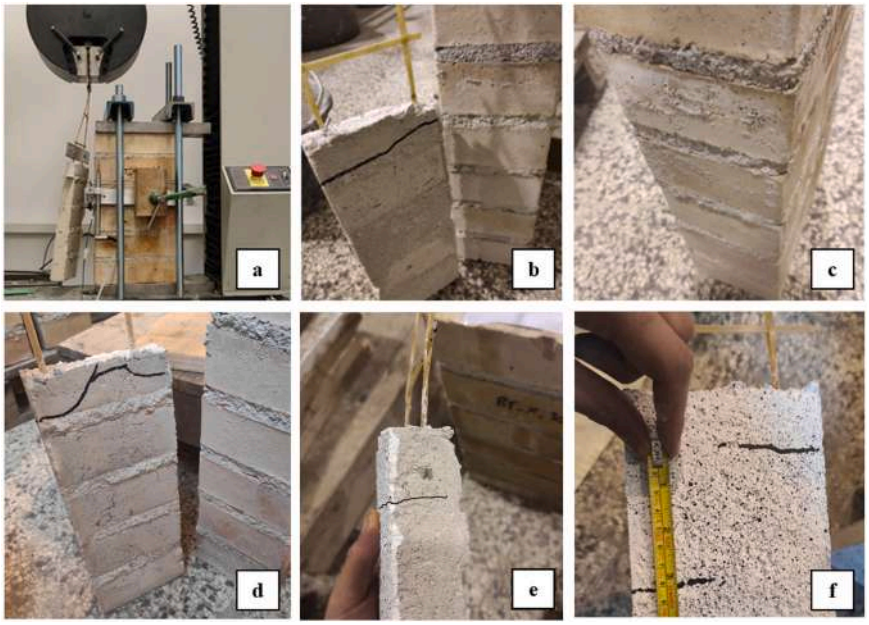

Fig. 5. Failure mechanism obtained from bond tests: detachment at the matrix-to-masonry interface and cracking in the upper portion of the matrix.

conventional strength defined by CNR-DT 215/2018 for FRCM systems. Considering the specimens of the 1st set values of $\sigma_{deb,x} = 417$ MPa and $\sigma_{deb,y} = 370$ MPa were obtained in the weft and warp direction, respectively.

3. Centred and out-of-plane eccentric axial compression tests

3.1. Setup

Two uniaxial compression tests and one out-of-plane eccentric compression test on slender columns were performed. Three specimens with dimensions 230 × 115 × 1200 mm^3 consisting of a single row of clay solid bricks were built. A concrete beam 50 mm thick was inserted at the base to distribute the load and to avoid directly loading the two layers of plaster. The geometry of the specimens was chosen to evaluate the effect of the CRM on the compressive instability of the samples. The possible buckling induced by the slenderness and the eccentricity of the vertical loads is a critical factor in the definition of the load-bearing capacity of walls. The samples had a slenderness $\lambda = H/t$ slightly higher than 10, which is a value compatible with solid brick walls of real structures. The reduced length of the specimens, equal to 230 mm, was chosen to obtain a compressive strength lower than 500 kN, the maximum value achievable by the testing machine adopted for the tests. Two panels were reinforced with two sides of CRM, while a panel was reinforced on a single side. A fourth panel had been made keeping it unreinforced for comparison but it was not tested since it was damaged during the assembly into the test setup. The walls were cured in the external area of the laboratory for 90 days before the application of the reinforced plaster, and then for another 90 days after the application of CRM before testing. The application of the CRM was carried out once wall surfaces were cleaned from dust and wet. In the three samples tested no connectors were used, therefore the connection between masonry and mortar was achieved by the adhesion of the masonry-mortar interface. The choice to not use connectors was linked to the significant slenderness of the panels: the execution of holes and the percussion application of the connectors would have damaged the specimens. Two different modalities of application of the vertical load were considered with the aim of evaluating the effect of compression eccentricity on the out-of-plane behaviour of the wall. The first two specimens, namely *COMP_2_c* and *COMP_1_c*, were characterised by a centred load (zero eccentricity). To uniformly apply the uniaxial compression on the upper surface of the panel, a thin concrete capping was made and a 400 × 100 x 20 mm^3 steel plate was inserted at the top of the panel, between the upper section and the testing machine. The steel plate also allowed the application of the vertical load only to the masonry cross-section, keeping unloaded the CRM layers, so that the transfer of the load between masonry and plaster could be achieved only through the development of tangential stresses at the interface. The choice of loading only the masonry cross-section was made to reproduce the loading transfer in a real scenario, where, after the application of the CRM, any load increase is likely directly applied to the panel by the floor and by the upper portion of the wall, while the reinforcement is loaded by shear stresses at the interface. The pre-load acting on the walls before the application of the CRM was not reproduced in the experimental setup. The obtained setup simulates a scenario in which the reinforcement is not rigidly connected at the base (at the foundation or at inter-storey level) due to the presence of the concrete beam. A representation of the setup used for the two specimens with centred load is shown in Fig. 6.

The third sample *COMP_2_ecc* was characterised by 2 layers of CRM and the vertical load was applied eccentrically on the top section of the panel. The vertical load was applied with an eccentricity of $t_m/4$, being t_m the thickness of the panel. The value of the eccentricity has been assumed equal to the maximum value provided by the Italian Building Code [15] for load-bearing walls characterised by a slenderness greater than 10. To avoid horizontal displacements of the top section due to the resulting bending related to the eccentricity, a steel roller has been welded to the upper plate and has been inserted into an additional steel plate connected to the piston of the testing machine (Fig. 7a,b). Anyway, the roller allowed the free rotation of the top section. The out-of-plane horizontal displacement of the base section was also prevented through the insertion of an additional steel plate connected to the testing machine and contrasted with the concrete beam placed at the base of the panel. The resulting static scheme of the panel is a column restrained at

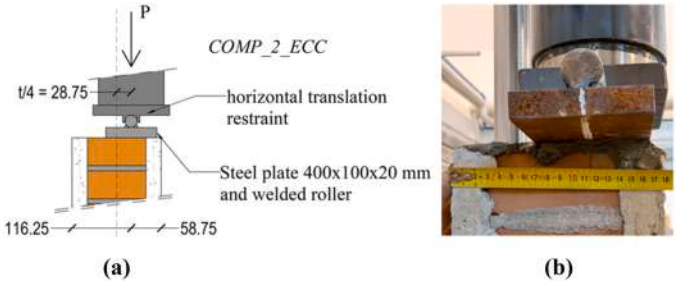

Fig. 7. Compression test with eccentric load COMP_2_ecc: (a), (b) hinge in the top section.

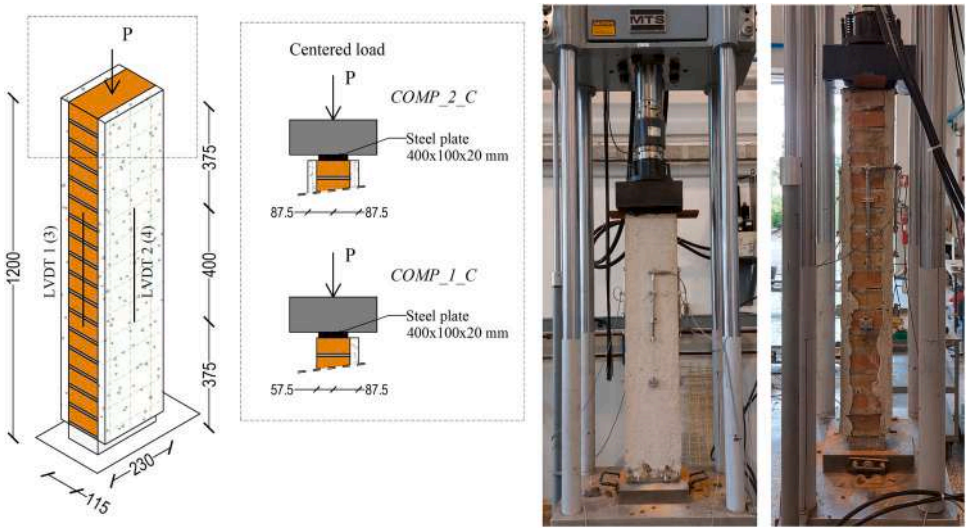

Fig. 6. Compression tests with centred load COMP_2_C and COMP_1_C.

the base and simply supported on top with a cylindrical hinge subject to an eccentric compression load (see Fig. 10 c). Differently from the two uniaxial compression tests, in this case, the load was applied at the top both to the masonry and to the mortar layer in contact with the steel plate, while at the base the support reaction was still applied to the panel only through the concrete beam.

The vertical load was applied in displacement control with a rate of 0.01 mm/s. According to EN 1052–1 [25] the compressive load was applied in three equal steps until reaching half of the maximum expected force. After reaching half of the expected compression strength, the load was increased until failure. Four strain gauges with a gauge length equal to 400 mm have been applied to measure vertical displacements and relative axial strains: in the double-sided reinforced panels, the LVDT 1 and 3 have been placed on the lateral faces (i.e., not reinforced) of the panels to measure masonry deformations, while LVDT 2 and 4 were applied to the plaster. In this way, it was possible to measure any difference between masonry and plaster displacements due to the shear deformability of the masonry-mortar interface. In the case of single-side CRM, only LVDT 4 was applied to the plaster. Table 4 summarises the characteristics of the specimens.

3.2. Results

The results are shown in terms of compressive stress σ_m calculated by dividing the applied load by the masonry cross-section (115 × 230 mm^2) and axial deformations ε_m. The axial strains of the masonry were calculated by dividing the displacement measured by the strain gauges directly connected to the bare panel (1 and 3 in the case of two-sided reinforcement and 1,2 and 3 in the case of single-sided reinforcement) by their gauge length. The output σ_m - ε_m diagrams are shown in Fig. 8.

The specimen *COMP_2_c* showed a peak load $P_u = 297$ kN, which corresponds to a compressive strength of 11.20 MPa. The elastic modulus was calculated as the secant value at one-third of the ultimate load and was equal to $E_m = 5915$ MPa. During the test the detachment at the CRM-to-masonry interface was observed (Fig. 9): the detachment began in the upper portion of the panel at a load of about 70 kN and the CRM layers completely detached from the masonry at a load of 150 kN. After this moment, the load was applied only to the masonry cross-section along the entire height; the column failed due to compressive crushing of the masonry, characterised by typical vertical cracks.

The elastic modulus was greater (+22%) than the Young modulus measured from characterisation tests. The result was related to the presence of coating layers since the elastic modulus was evaluated at a third of the ultimate load when the complete detachment of the plaster had not yet occurred. The specimen *COMP_1_c* has shown a behaviour quite similar to the previous one. The maximum compression load reached was $P_u = 287$ kN and the elastic modulus was equal to $E_m = 5980$ MPa. Even in this case, the detachment at the CRM-to-masonry interface was observed at a load of about 150 kN and, after the detachment, the failure was caused by the compressive rupture of the masonry. The similar response characterising the two specimens, regardless of the number of CRM layers, showed little influence of the coating in the uniaxial compression response of panels loaded by a centred load applied to the masonry cross-section only. A similar result was observed by Donnini et al., 2021 [18] for brick and tuff masonry panels. The Young modulus was slightly higher than that obtained in the case of 2-sides reinforcement due to the different detachment propagation since in the one-side reinforced specimen the detachment at the top of the panel was less evident. To investigate the influence of the reinforcement in the case of out-of-plane bending, a panel with a prescribed compression eccentricity was tested; the eccentricity was set equal to 28.75 mm, corresponding to ¼ of the panel thickness. The obtained peak load was equal to 191 kN, lower than that obtained for the centred load due to the out-of-plane effects. Differently from the previous specimens, the collapse was not achieved due to the crushing of the masonry, but by the instability of the panel, as shown in Fig. 10 b. An initial detachment of the mortar placed on the compressed side was observed (Fig. 10a) at a load of about P_{detch}= 133 kN. When the layer placed on the loaded side detached, a sudden decrease of the load was observed and the layer placed on the opposite side, remaining adherent, began to show tensile deformations and contributed, due to the tensile strength of the mortar and mesh, to limit the instability of the panel. The tensile reaction of the plaster layer placed on the unloaded side was experimentally observed by the trend of strains during the test: as shown in Fig. 11, where the loading trend during the test together with the trend of axial strains recorded by transducers is plotted, after the detachment of the compressed coating at about 500 s from the beginning of the test, the strain measured by LVDT 4 changed sign showing elongation. The collapse

Table 4
Specimens considered for uniaxial compression tests.

Id Tests	Reinforcement	t_{pl} [mm]	t_m [mm]	H [mm]	Eccentricity [mm]
COMP_2_c	2 sides	30 + 30	115	1200	0
COMP_1_c	1 side	30	115	1200	0
COMP_2_ecc	2 sides	30 + 30	115	1200	28.75

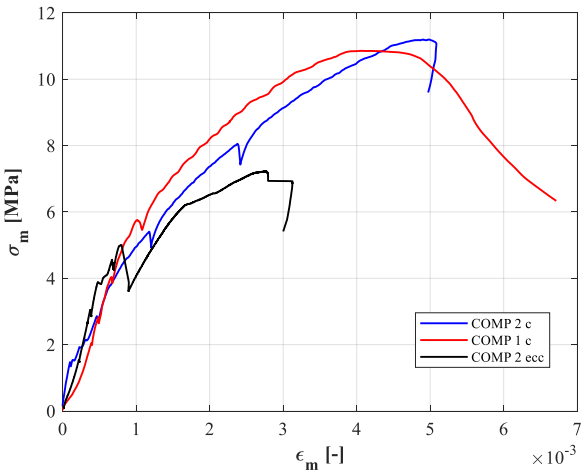

Fig. 8. Compression response: stress and strain are referred to the masonry cross-section (230x115mm^2).

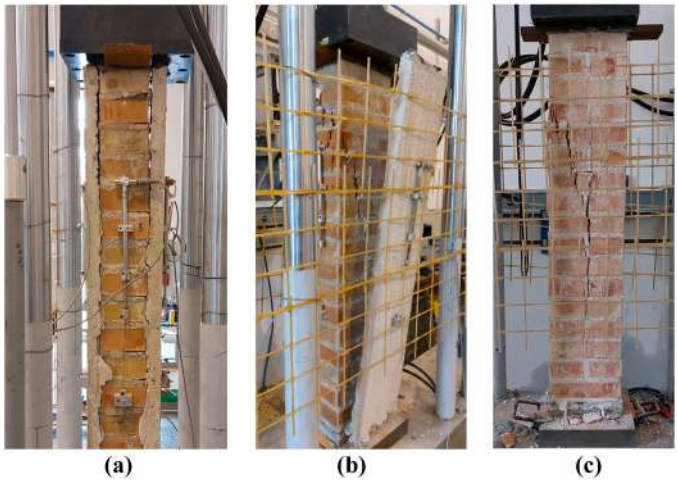

Fig. 9. COMP_2_c: (a) initial detachment at the mortar-support interface (P ≈ 70 kN); (b) complete detachment (P_{detach} ≈146 kN); (c) compressive rupture of the masonry with typical vertical cracking (P_u = 297 kN).

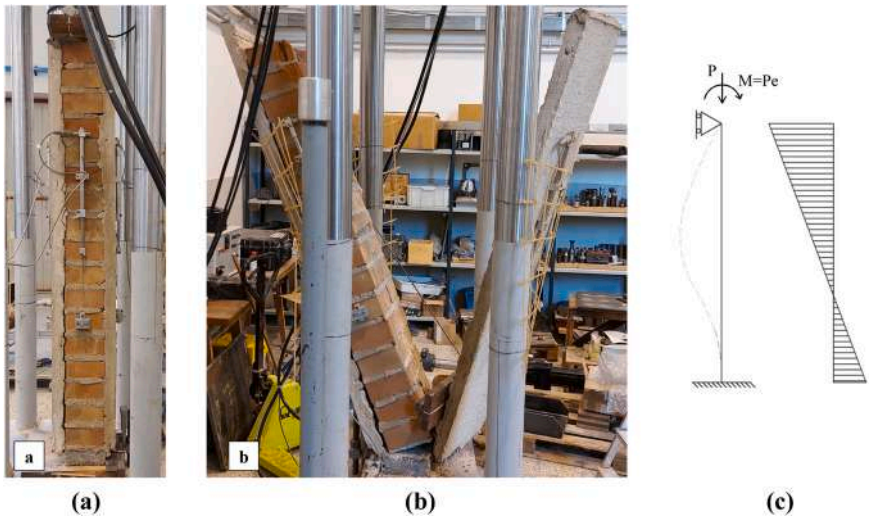

Fig. 10. COMP_2_ecc: (a) detachment of the compressed CRM layer; (c) bending failure mechanism with final detachment; (c) static scheme of the panel eccentrically loaded.

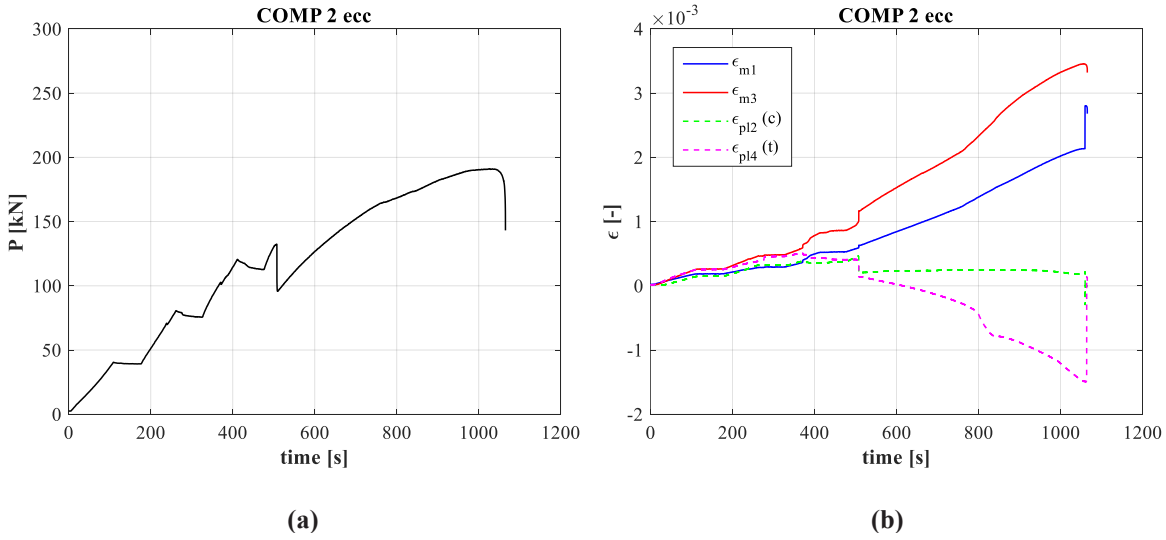

Fig. 11. (a) Loading trend during the test; (b) trend of strains (positive values compression, negative values tension).

occurred due to the debonding of the tensile mortar layer and the crushing of the masonry in the upper section.

Table 5 summarises the results in terms of compressive load registered at the moment of the detachment P_{detach}, peak load P_u, masonry compressive strength $f_{c,m}$ and masonry Young modulus E_m.

4. Shear-compression tests

Shear compression tests are typically used to define the lateral response of unreinforced masonry walls [32–35]. These tests consist of the application of a prescribed vertical load on the wall simulating the actual gravitational loads, kept constant during the test, together with the application of a horizontal load, usually imposed in monotonically or cyclic displacement control, at the top of the panel. The static schemes commonly used are double-bending, in which the rotation of the top section of the wall is restrained, representing a wall characterised by strong spandrels, or cantilever, in which a free rotation is imposed at the top, representing a wall characterised by weak spandrels. The axial load ratio p (i.e., the ratio between the axial stress applied at the beginning of the test and the compressive strength of the masonry) strongly influences the response, leading to a flexural failure characterised by rocking for panels with low compression or shear failure for panels with medium-high compression levels [35,36]. In this work, quasi-static cyclic shear-compression tests were carried out on solid brick masonry panels with or without CRM, to assess the reinforcement efficiency on the in-plane seismic behaviour. A cantilever static scheme with intermediate support at about half of the wall height was considered. The middle-height support allowed to simulate the possible presence of a spandrel in the lower portion of the wall and to evaluate the effect of the GFRP grid anchoring on the flexural response.

Table 5
Compression test results.

Id Tests	P_{detach} [kN]	P_u [kN]	$f_{c,m}$ [MPa]	E_m [MPa]
COMP_2_c	146	296.1	11.20	5915
COMP_1_c	150	287.1	10.86	5980
COMP_2_ecc	133	190.9	7.22	7677

4.1. Setup

Six panels made of solid clay brick masonry with dimensions of 1000 × 1250 × 240 mm^3 were built and were equipped with a 50 mm concrete beam at the base to simplify their movements. Four of the six panels were reinforced with the CRM system: five pre-drilled through-holes were made in each reinforced wall, and then the GFRP grid was applied on the reinforced faces, arranging the weft yarns in the horizontal direction; subsequently, steel helical connectors were inserted and bent over the grid, applying 5 connectors for each specimen; finally, the lime-based mortar was applied with a thickness of about 30 mm per side. The surfaces of the panels were cleaned from any dust and were wet before applying the mortar. The panels were cured in the external area of the laboratory for 120 days before the application of the plaster; once the plaster was applied, they were cured for another 60 days before testing. Two walls were kept unreinforced as a reference (*SC_URM_01* and *SC_URM_02*), two walls were reinforced with two layers of CRM applied on both faces (*SC_RM_2_01* and *SC_RM_2_02*), and the last two with one layer only applied on a single side (*SC_RM_1_01* and *SC_RM_1_02*). The application of the reinforcement system and a sketch of unreinforced and reinforced panels are shown in Fig. 12.

The six panels were tested in shear-compression considering a cantilever static scheme with a free height of the wall equal to h_{eff} = 745 mm. The test setup was characterised by a self-balanced steel frame structure. A representation of it is shown in Fig. 13. Three HEB 320 beams provided the base support of the panel (mark 1 in Fig. 13). The compression load was applied through a vertical mechanical actuator and maintained constant during the whole test (mark 2). The vertical actuator was connected to the steel structure through two columns HEB 240 and two rigid C-shaped beams. The horizontal displacement was applied through a horizontal actuator, with a maximum displacement capacity of ± 75 mm and a maximum load capacity of 350 kN (mark 3). A HEB 280 beam was placed at the top section of the panel to uniformly apply the vertical load and to transfer the horizontal displacement (mark 4); the transfer of the horizontal force from the actuator to the wall was guaranteed by the presence of two L-shaped profiles welded to the top beam and by the friction between the beam and the upper surface of the wall. To restrain lateral out-of-plane displacements of the panel, an adjustable restraint system was designed, consisting of two UPN 160 beams on which adjustable steel plates have been fixed and placed in contrast with the top beam placed above the wall (mark 5). Teflon sheets were placed between the top beam and the out-of-plane restraining system to avoid frictional resistance for horizontal movements during the test. Regarding the static scheme, the effective height of the panels was reduced by introducing a contrast system at about their middle height: the restraint was built through two metal plates with dimensions 300x600x50 mm^3 (mark 6) forced against the panel through two M24 bolts (mark 7). The bolts were connected to two horizontal beams HEB 320 and were preloaded before the beginning of each test. The middle-height support was inserted since the applied compressive stress together with the cantilever static scheme would have induced a failure by rocking considering the overall height of the walls (namely, 1250 mm). In the case of rocking around the base section, the assessment of the CRM efficiency would not have been possible, being the grid not anchored at the base of the walls. The vertical and the horizontal loads were transferred from the upper beam to the panel using two possible strategies, thus two sets of tests were carried out: in the first set of tests (*SC_URM_01*, *SC_RM_2_01* and *SC_RM_1_01*) a rubber sheet of size 1000 × 240 × 20 mm^3 was placed above the panel, between the top beam and its upper face, to avoid stress concentrations and, in the case of reinforced panels, to apply the vertical load only to the masonry without directly loading the CRM layers (Fig. 14, left); differently, in the second set of tests (*SC_URM_02*, *SC_RM_2_02* and *SC_RM_1_02*) a thin concrete layer about 5–10 mm thick was inserted instead of the rubber sheet to avoid stress concentrations at the top; in this case, both the wall and CRM layers were loaded by the vertical actuator (Fig. 14, right). The main difference between the two sets lies in the modality of application of the horizontal load: in the first case, due to the negligible tangential stiffness of the rubber, the horizontal load was applied concentrated at the upper corners of the panels through the contrast between the L-shaped profile welded to the top beam and the masonry; in the second case, the horizontal load could be assumed as distributed on the top surface thanks to the presence of the cement layer that, together with the friction, joined the top beam and the head of the wall. The application of the vertical reaction only to the masonry without directly loading the CRM layers was guaranteed at the base section of the specimens by the presence of the 50 mm concrete base. The concrete layer at the top section of the walls in the second set was laid using a quick-setting cement type *Geolite 40* (compressive strength ≥ 45 MPa, Young modulus ≥ 20 GPa, according to the manufacturer's datasheet) to have a short hardening time, necessary to perform the test shortly after placing the panel in the test bench. The monitoring of displacements during the test was guaranteed by four diagonal extensometers placed on the faces of the specimens. The displacement at the top of the panels was recorded using a measuring laser positioned at the top of each panel (Laser 1 in Fig. 13). A second laser (Laser 2) was used to monitor the displacements of the HEB 320 beam at mid-height and to verify the efficiency of the support. An additional extensometer (LVDT 5) was placed at the middle-height section of the masonry in order to measure the actual base displacement of the panel linked to the deformation of the contrast beams. Finally, the vertical and horizontal loads were recorded by the loading cells of the two actuators, together with

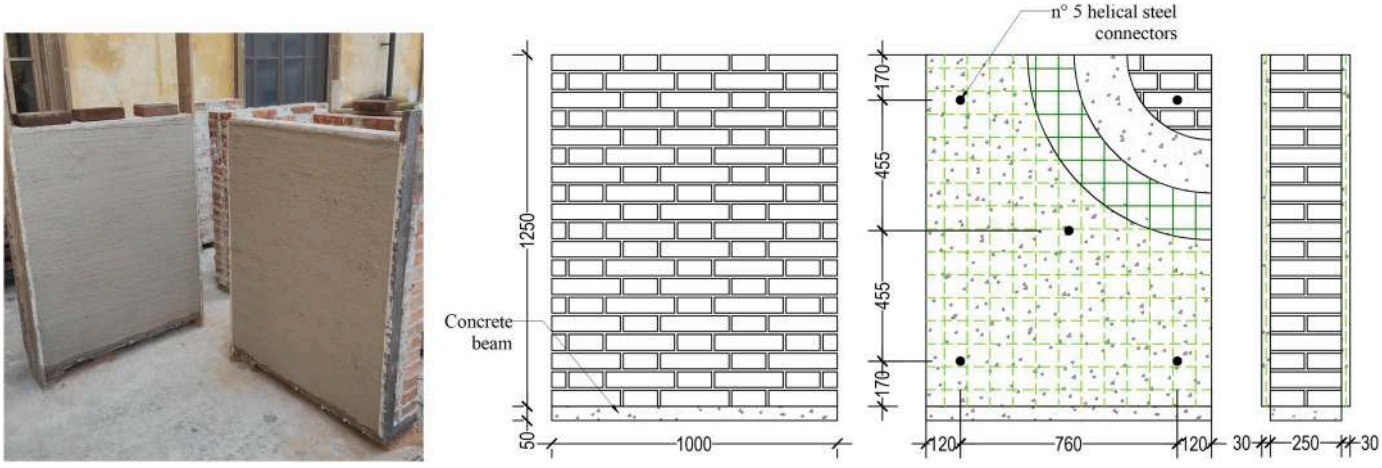

Fig. 12. Application of CRM on solid clay brick masonry walls and geometry of unreinforced and reinforced walls.

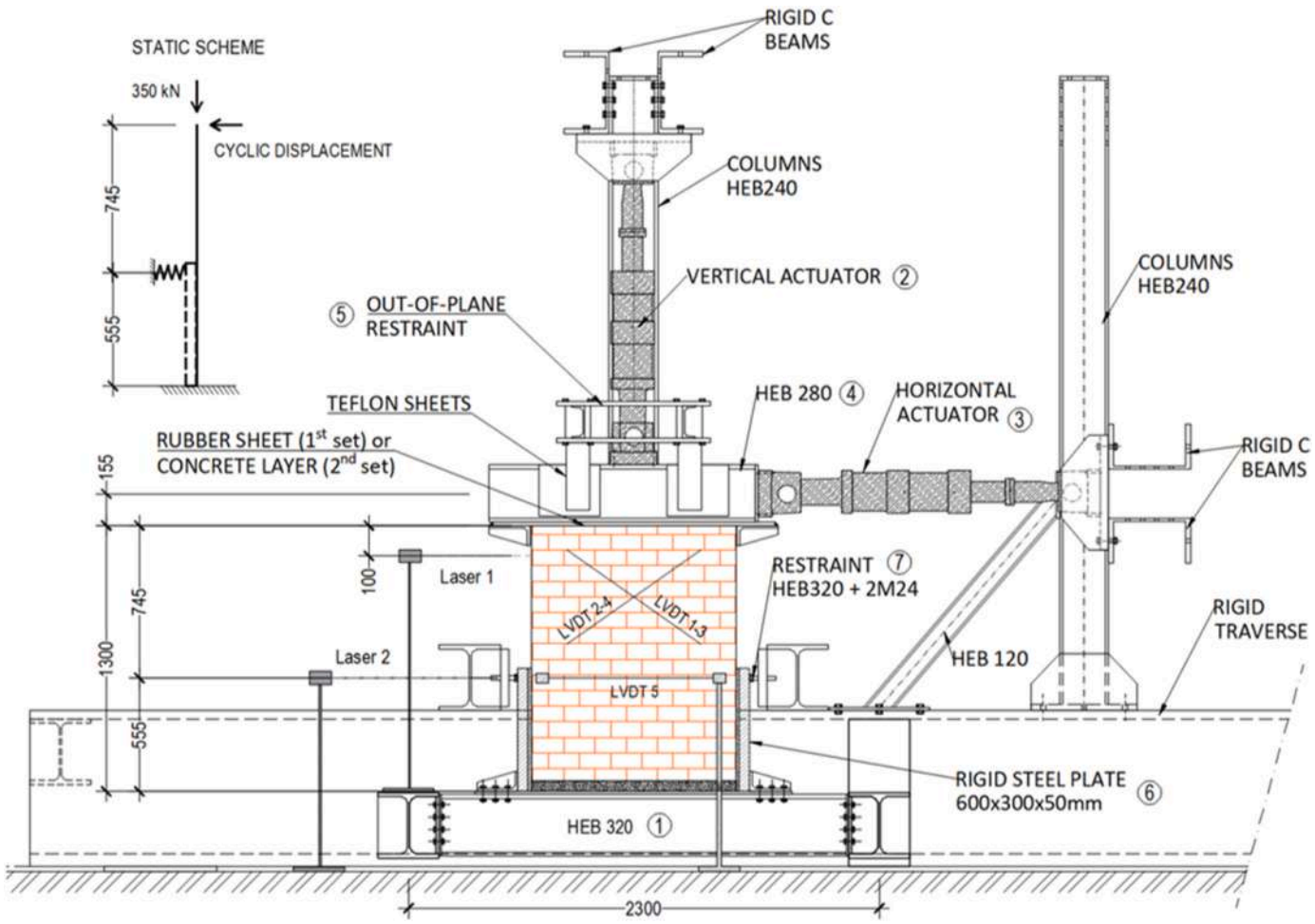

Fig. 13. Longitudinal view of the setup used for the shear-compression tests.

Fig. 14. On the left, 1st set: rubber sheet on the top of the wall; on the right, 2nd set: concrete layer on the top.

the vertical and horizontal displacements. Tests were carried out with the application of the vertical load equal to 350 kN at the beginning of each test using a loading ramp about 400 s long and then kept constant during the cyclic procedure. This load corresponded to a compression stress of about $\sigma_0 = 1.45$ MPa and to a compressive ratio $p = \sigma_0/f_{c,m} \approx 0.11$, where $f_{c,m}$ is the compressive strength of the masonry derived from mechanical characterisation tests. Then, the horizontal quasi-static cyclic action was applied in displacement control, with a rate equal to 0.20 mm/s and at increasing drift considering the following procedure: $\theta = u/H$ [%] = 0.025–0.05–0.10–0.15–0.2–0.3–0.4–0.6–0.8–1.0–1.5–2.0–2.5–3.0–3.5–4.0, where H was the total height of the wall, namely 1250 mm and u the imposed horizontal displacement.

Specimens were named according to the notation *SC_X_n_Y*, where -*SC* indicates Shear Compression tests, -*X* the presence or absence of the reinforcement (*URM* unreinforced masonry, *RM* reinforced masonry), -*n* the number of layers of CRM applied on reinforced walls (*1* in case of application on a single side and *2* in case of double-side), -*Y* the test setup, namely *01* in case of rubber sheet applied at the top and *02* in case of the concrete layer. A summary of specimens is provided in Table 6.

Table 6
Identification of samples used for shear-compression tests and their main characteristics.

ID Test	Reinforcement	t_{pl} [mm]	Load application	N [kN]
SC_URM_01	no	0	Rubber sheet	350
SC_RM_2_01	2 sides	30 + 30	Rubber sheet	
SC_RM_1_01	1 side	30	Rubber sheet	
SC_URM_02	no	0	Concrete layer	
SC_RM_2_02	2 sides	30 + 30	Concrete layer	
SC_RM_1_02	1 side	30	Concrete layer	

4.2. Results

In the following, the results of the shear compression tests are provided, considering at first the results of the first set of specimens,

performed using a rubber sheet to transfer the load at the top, and then the second sets, in which the transfer was guaranteed by a concrete layer. Results are provided in terms of capacity curves, having on the *y*-axis the horizontal load F_h measured by the horizontal actuator and on the *x*-axis the displacement of the top section with respect to the middle-height section, δ. The displacement δ has been calculated as the difference between the displacements measured at the top of the panel through Laser 1 and the displacement of the middle-height restrained section measured by the strain gauge LVDT 5. The results of shear-compression tests of the first set of specimens are shown in Fig. 15 a-d in terms of capacity curves. In Fig. 16 observed failure mechanisms of unreinforced and reinforced masonry are shown. The unreinforced wall was characterised by a rocking behaviour, overturning around the corners of the middle height cross-section (Fig. 16 a). After several cycles characterised by rocking, a diagonal crack appeared at the centre of the wall and a sudden strength decrease was observed (Fig. 16 b). The cyclic response (Fig. 15a) showed the typical S-shaped curve characterising rocking, with a high displacement capacity and negligible energy dissipation. The registered peak shear strength, calculated as the average value between the positive and negative cycles, was equal to 176 kN, and the ultimate drift to about 19 mm. The two-sided reinforced wall *SC_RM_2_01* reached the peak load once the first diagonal crack appeared on both sides of the reinforcement mortar (Fig. 16 c). Once cracks appeared, the detachment at the masonry-to-mortar interface occurred and sliding of the masonry with respect to the two CRM layers was observed (Fig. 16 d). The detachment at the masonry-mortar interface produced a significant decrease in shear load and a significant increase in the lateral displacements registered in the cycles following the cracking. In the end, the failure of masonry was observed, including diagonal cracking and toe-crushing. The presence of steel connectors ensured the integrity of the panel despite the significant damage. Conversely, the detachment of the mortar has shown the low contribution of the connectors in the shear-stress transfer mechanism, as also observed from the results of bond tests. The strength was equal to 198 kN and the registered ultimate displacement to 19.5 mm; however, it must be noted that this ultimate displacement was reached with a significant decrease in the horizontal load, of about 35%. Single-sided reinforced specimen *SC_RM_1_01* showed quite similar behaviour: the panel was characterised by an almost linear response until the first diagonal cracks appeared. Diagonal cracks occurred at the same time in both the plastered and the unreinforced sides. After the opening of the diagonal cracks, the detachment at the masonry-to-mortar interface was observed in the loaded corner of the wall. The registered peak load was 190 kN and the ultimate displacement was 15.5 mm, showing a

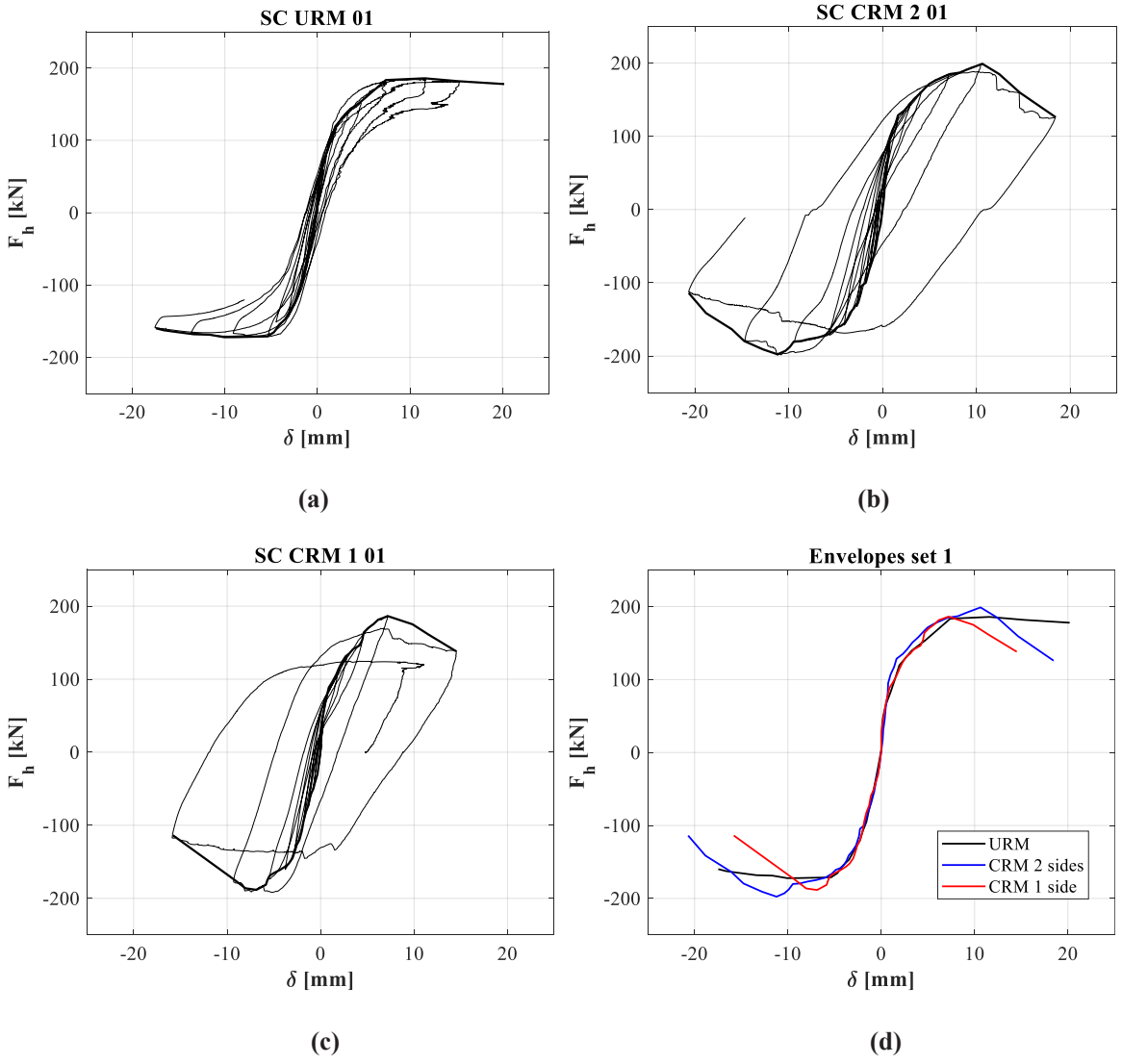

Fig. 15. Results of the 1st set: (a) cyclic response and envelope of the unreinforced wall, (b) 2-sided reinforced wall, (c) 1-sided reinforced wall, (d) comparison between envelopes.

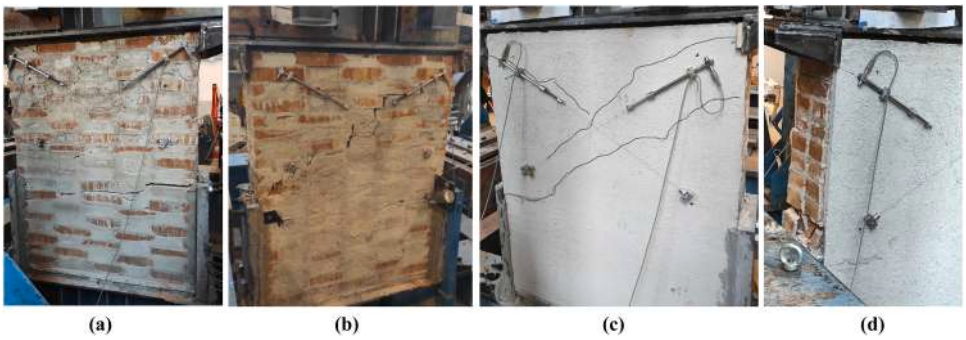

Fig. 16. (a) Rocking of URM specimen and (b) diagonal cracking at the end of the test; (c) diagonal cracking in the mortar and (d) detachment of the mortar from the support in the specimen SC_RM_2_01.

reduction of the drift capacity with respect to the unreinforced wall. A comparison between the envelope response is provided in Fig. 15d.

Regarding the second set of specimens, characterised by a more uniform application of the horizontal load at the top of the wall, the results are shown in Fig. 17 a-d in terms of capacity curves and Fig. 18 in terms of observed failure mechanisms. The unreinforced panel *SC_URM_02* collapsed due to mixed failure related to shear-sliding along mortar joints and a progressive rocking/toe-crushing in the corners (Fig. 18 a). The hysteretic response showed also in this case the typical S-shaped curve characterising the rocking behaviour, but with a higher internal area related to the energy dissipation provided by the sliding along the mortar joints. The peak load was equal to 173 kN and the registered ultimate displacement to 19 mm. The two-sided reinforced wall *SC_RM_2_02* showed a transition from rocking to shear failure, by

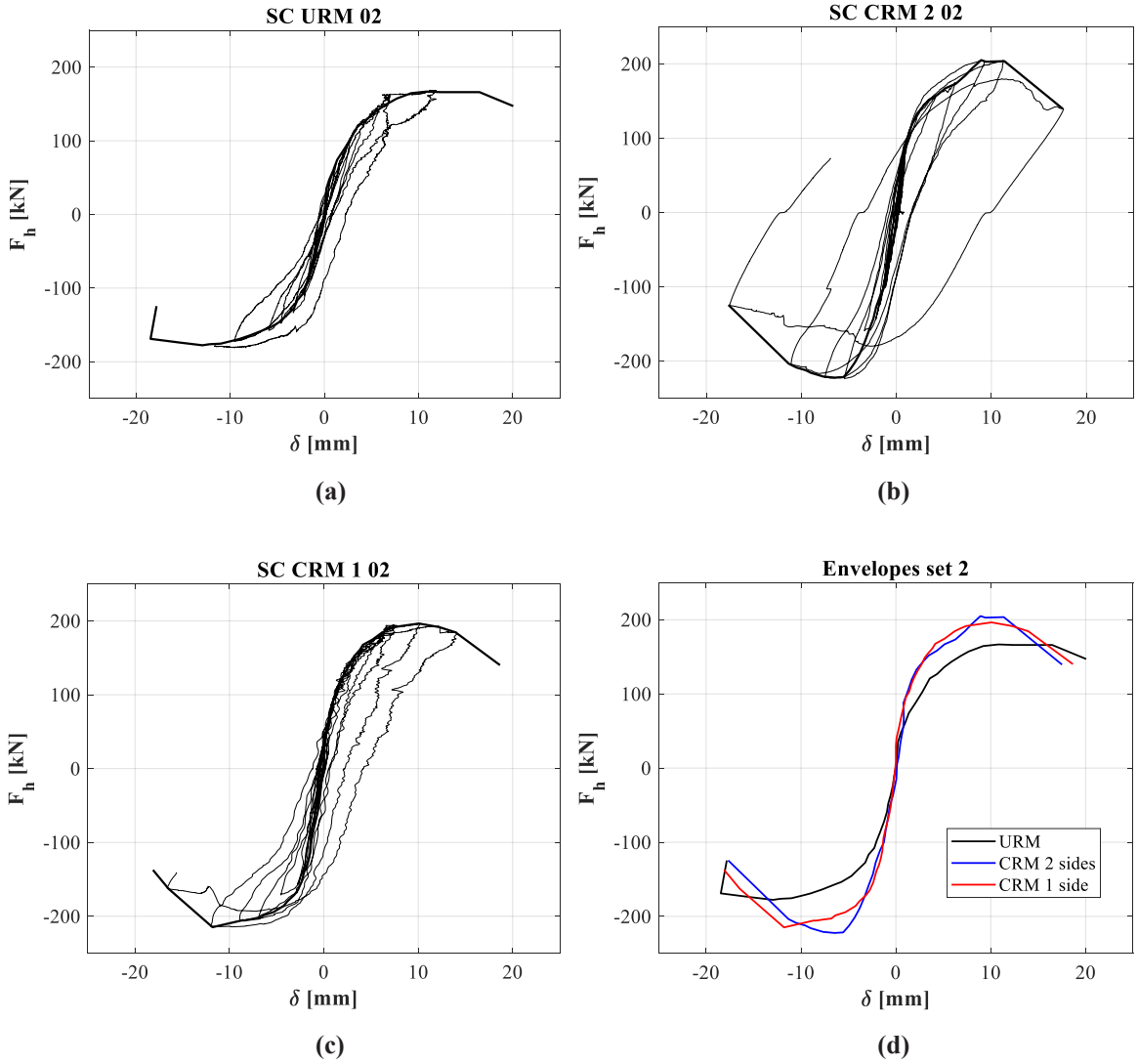

Fig. 17. Results of 2nd set: (a) cyclic response and envelope of the unreinforced wall, (b) of the 2-sided reinforced wall, (c) of the 1-sided reinforced wall, (d) comparison between envelopes.

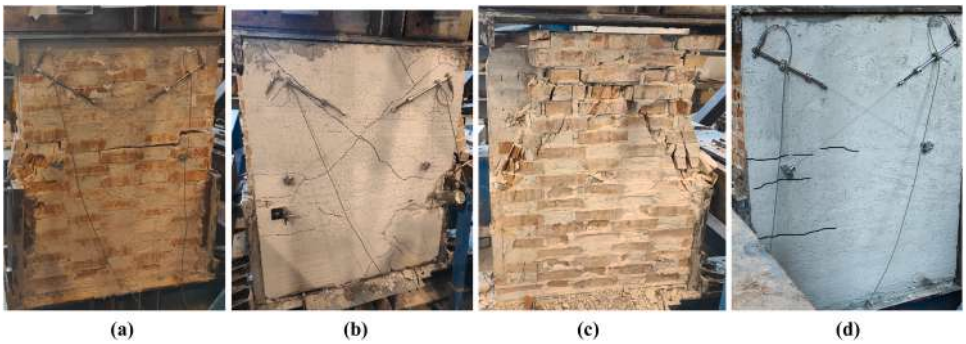

Fig. 18. (a) Flexural failure of specimen SC_URM_02; (b) Diagonal cracking in the plaster and (c) in the masonry at the end of the test SC_RM_2_02; (d) rocking failure of the specimen SC_RM_1_02.

developing diagonal cracks on both plastered sides (Fig. 18 b). After the cracking, the detachment of the mortar was also observed, which started in the upper portion of the panel and then extended to the entire surface of the wall placed above the middle-height restrain; in the lower portion of the wall the plaster remained bonded to the masonry until the end of the test, thanks to the confinement effect ensured by the rigid steel plates. At the end of the test, the plaster was removed from the wall to observe the cracking of the masonry, showing a rupture due to diagonal cracking (Fig. 18 c). A wide horizontal crack was also observed in the middle height restrained section, where the vertical yarns prevented the possible rocking of the wall around the corners. The hysteretic response showed damaging behaviour, with a progressive loss of stiffness related to diagonal cracking and a high energy dissipation. However, a sudden load decrease and displacement increase have been observed in the cycles after the occurrence of detachment. The lateral peak load was equal to 214 kN and the registered ultimate displacement to 17.6 mm. Finally, the specimen *SC_RM_1_02* was characterised by a failure mechanism similar to that of the unreinforced wall since the presence of the plaster on only one side did not completely prevent the rocking. The rupture occurred by the shear-sliding of bricks along the middle-height mortar joints, accompanied by a rocking; the plastered side showed some horizontal cracks at the base cross-section, proving its influence in postponing the flexural rupture (Fig. 18 d). The detachment of the plaster from the masonry was in this case observed in the central portion of the panel and was caused by the significant tangential stresses developed in the interface for the transfer of shear and axial stresses. The cyclic response showed a hysteretic behaviour quite similar to that of the unreinforced specimen; however, the peak load and the stiffness recorded were greater than those of the URM, while the ultimate displacement was about the same. The lateral peak load and the ultimate displacements were equal to 204 kN and 18.5 mm, respectively.

Table 7 summarises the results of shear-compression tests in terms of failure mechanism (namely, *R* means rocking; *DC* diagonal cracking; *SS* shear sliding), peak strength V_{max}, stiffness *K* (evaluated as the secant stiffness at 0.70 V_{max}), displacement capacity δ_{max}, which is the maximum displacement reached at the end of the tests, and δ_u calculated at 80% V_{max}; also the ultimate drift $\theta_u = \delta_u / H_{eff}$ is provided. All the aforementioned parameters have been calculated referring to the envelope quantities. The strength, stiffness and displacement capacities were evaluated for both the positive and negative cycles and the output values have been obtained from their average. In addition, the comparison between reinforced and unreinforced samples is provided in terms of amplification coefficients of strength $\alpha_V = V_{max,R}/V_{max,URM}$, stiffness $\alpha_k = K_R/K_{URM}$ and ultimate displacement $\alpha_{\delta max} = \delta_{max,R}/\delta_{max,URM}$ or $\alpha_{\delta u} = \delta_{u,R}/\delta_{u,URM}$ ensured by the application of CRM.

The application of reinforced plaster led to an increase in shear strength and lateral stiffness and a slight reduction in displacement capacity. Despite the similar failure mechanism observed in both test sets, the CRM effect was significantly affected by the modality of application of the horizontal load. In the first set of tests, the effect of the coating was limited both in terms of strength and stiffness by the concentrated application of the load at the corners, which produced a significant concentration of tangential stresses at the masonry-CRM interface inducing a premature detachment. Furthermore, the reduction of the ultimate displacement, observed in both sets, was related to the transition from the rocking failure mechanism characterising the unreinforced specimens to the diagonal cracking. However, it is worth noting that the minimum ultimate drift $\theta_u = \delta_u / H_{eff}$ of the two-sided plastered wall was 2.05%, about three times higher than the ultimate drift usually expected in an unreinforced masonry wall failing by shear [33]. Besides the effect on stiffness, resistance, and ultimate displacement, the capacity to dissipate energy is a crucial factor in the seismic response of structures. The integrity of a building when subjected to an earthquake depends on its ability to dissipate the energy input from the ground acceleration. From experimental tests was possible to calculate the energy dissipated by walls before and after the retrofitting. The energy dissipated in a cycle was calculated as the area enclosed by the hysteretic cycle and then the cumulative dissipated energy was derived by summing the dissipation in consecutive load-displacement loops throughout the tests. Fig. 19 a, b provide the cumulative dissipated energy against the progressive increase of maximum lateral displacement for the two sets of shear compression tests. Regarding the first set, the energy dissipated by the specimens *SC_URM_01, SC_RM_1_01* and *SC_RM_2_01* were 4297 J, 7369 J and 10,847 J, showing a 71% and 152% increase in the capacity

Table 7
Results of shear compression tests in terms of failure mechanism, peak shear strength, secant stiffness, and ultimate displacement reached at the end of the tests and an 80% strength decrease. Amplification coefficients of masonry mechanical properties provided by the application of the CRM.

	FM	V_{max} [kN]	k [kN/mm]	δ_{max} [mm]	δ_u [mm]	$\theta_u = \delta_u/H$ [%]	α_V	α_k	$\alpha_{\delta max}$	$\alpha_{\delta u}$
SC_URM_01	*R/DC*	176	45	19.0	19.0	2.55	-	-	-	-
SC_RM_1_01	*DC*	188	50	15.5	13.6	1.81	1.07	1.11	0.82	0.72
SC_RM_2_01	*DC*	198	53	19.5	16.5	2.20	1.13	1.18	1.02	0.87
SC_URM_02	*R/SS*	173	40	19.2	19.2	2.57	-	-	-	-
SC_RM_1_02	*R*	204	55	18.5	16.9	2.25	1.18	1.39	0.97	0.88
SC_RM_2_02	*DC*	214	59	17.7	15.4	2.05	1.24	1.47	0.92	0.80

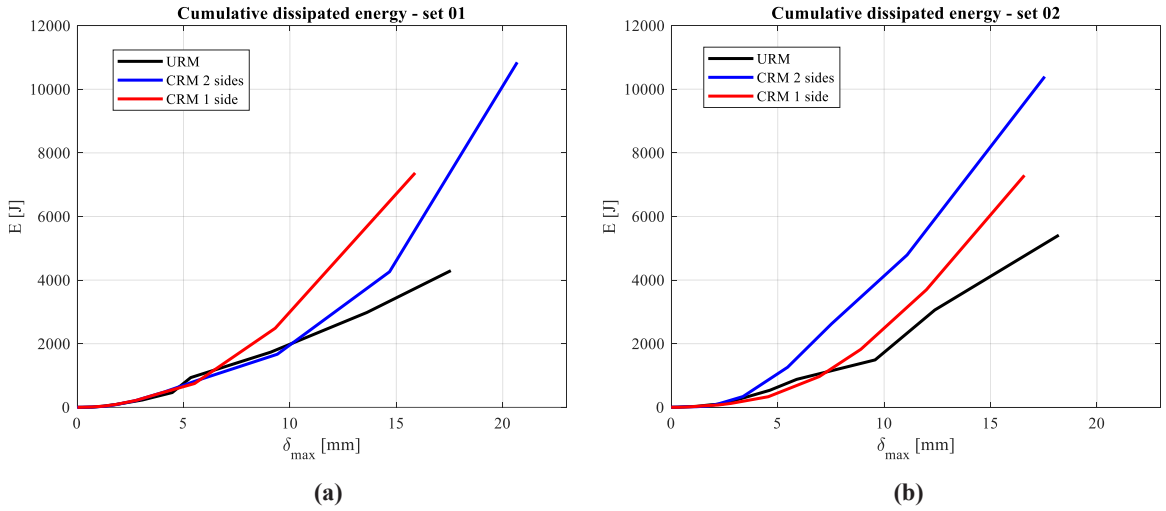

Fig. 19. Trend of cumulative dissipated energy against the progressive lateral deflection: (a) 1st set; (b) 2nd set.

of the wall to dissipate energy when strengthened on one or two sides, respectively. The high increase of dissipation in the plastered samples was related to the opening of diagonal cracks in the masonry and in the coating. Since in the single-sided reinforced wall the diagonal cracks opened in correspondence with a smaller displacement with respect to the symmetrically reinforced wall, for displacements lower than 15 mm the energy dissipated by the former was higher. Focusing on the second set of tests, the unreinforced specimen showed a higher energy dissipation since the rocking of the wall was also accompanied by sliding along the mortar joints. The application of reinforcement on two sides provided a significant increase in dissipated energy due to diagonal cracking; the application of CRM on just one side led to a lower increase since the rupture still occurred by rocking. The values of the total dissipated energy at the end of the tests for specimens *SC_URM_02, SC_RM_1_02* and *SC_RM_2_02* were 5401 J, 7295 J and 10,395 J, showing a 35% and 93% increase in the capacity of the wall to dissipate energy.

Starting from the energy dissipated in each hysteretic cycle, the equivalent viscous damping ξ has been calculated using the area-based approach, Eq. 1:

$$\xi_i = \frac{E_{dis,i}}{2\pi F_i \delta_{\max,i}}. \quad (1)$$

Where ξ_i is the equivalent viscous damping at the cycle -*i*, $E_{dis,i}$ is the area enclosed by the load-displacement curve at cycle -*i*, F_i and $\delta_{\max,i}$ the peak load and the maximum displacement occurred in the cycle -*i*. In Fig. 20 the trend of ξ is plotted at varying incremental ductility, calculated as the ratio between $\delta_{\max,i}$ and the limit elastic displacement of the bilinear curve obtained from the envelopes, $\delta_e = V_{max}/K$. The trend of the equivalent viscous damping of an elastoplastic oscillator is also plotted as the upper limit of damping. Considering the first set, the unreinforced panel showed equivalent damping of about 9%; CRM-reinforced specimens were characterised by an initial damping similar to that of the unstrengthened wall, whereas after the diagonal cracking the dissipation increased exponentially to values of 40% for the single-sided and 45% for the double-sided strengthened specimen. In the second set, the first hysteretic cycles of reinforced panels were characterised by lower damping since the damage was postponed due to the presence of the coating, and, after the appearance of the first cracks in the mortar, the equivalent damping increased exponentially. Maximum values of ξ equal to 12%, 39% and 23% have been obtained for unreinforced, two-sided reinforced and one-sided reinforced walls, respectively.

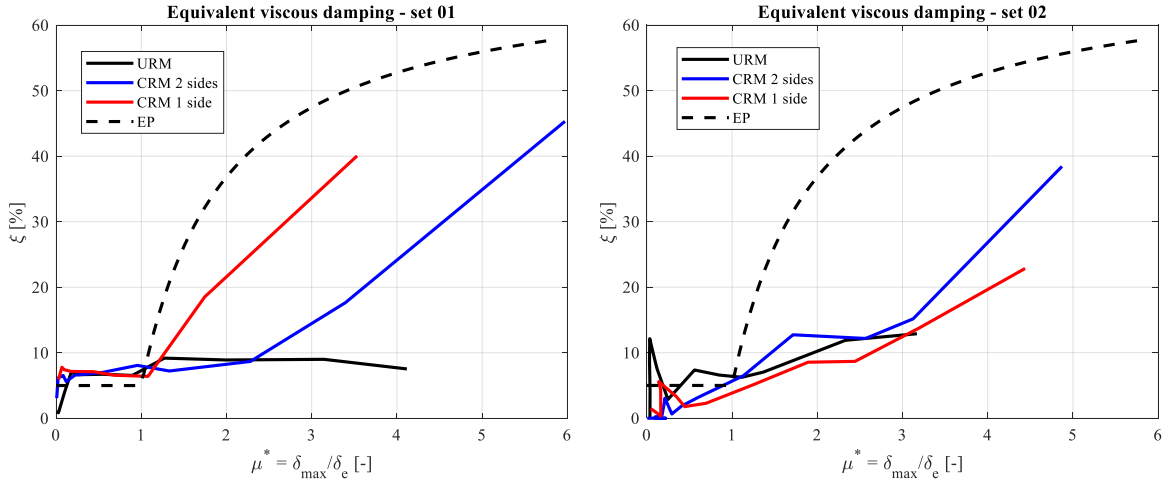

Fig. 20. Trend of equivalent viscous damping against ductility: (a) 1st set; (b) 2nd set.

5. Analytical estimation of strength

The calculation of the flexural strength and shear strength of the unreinforced panels was carried out using the analytical formulations proposed by the Italian Building Code [17]:

$$V_{\max,flex} = PL/2H_0(1-\sigma_0/0.85f_{cm}). \quad (2)$$

$$V_{\max,shear} = Lt_m \bullet 1.5\tau_0/b\sqrt{1+\sigma_0/1.5\tau_0}. \quad (3)$$

Being L= 1000 mm the length and t_m= 240 mm the thickness of the wall, H_0= 900 mm the distance between the mid-height restrained section and the point of application of the horizontal load, σ_0= 1.46 MPa the axial stress, f_{cm}= 14.40 MPa the masonry compressive strength, b= 1 a coefficient taking into account the aspect ratio of the wall and τ_0 the shear strength in the absence of compression of the masonry. From Eq. (2) a flexural strength equal to $V_{\max,flex}$= 172 kN has been obtained. This value is in good agreement with the experimental resistance of unreinforced specimens, which exhibited a strength of 176 kN (−2%) and 173 kN (−1%), respectively. For the calculation of the shear strength $V_{\max,shear}$, the value of τ_0 is not known since diagonal compression tests were not performed. Therefore, its value was estimated using the tabulated values proposed by the Italian Building Code [16] for solid brick masonry. Since the masonry employed in the work was characterised by a high compressive strength, the maximum value of 0.13 MPa was chosen and increased with the amplification coefficient provided for a masonry consisting of a good-quality mortar, namely $f_{c,mortar}^{0.35}$. The shear strength resulted in τ_0= 0.21 MPa. A value of $V_{\max,shear}$ = 179 kN was obtained. Referring to reinforced specimens, procedures for calculating the strength of CRM-reinforced panels have not yet been defined in the current Building Codes. The Guidelines released for FRCM consider the contribution of the system in increasing the flexural strength of a wall by calculating the compression-bending strength of the composed masonry-textile cross-section, while for the shear failure, the contribution of the FRCM is taken into account by summing to the unreinforced strength the contribution provided by the tensile strength of the textile mesh. However, as shown in the literature [18], [37,38], due to the significant thickness of the coating, the contribution of CRM in terms of shear strength is mainly related to the tensile strength of the plaster, while the mesh ensures the ductility of the panel once diagonal cracking occurs. In [3], the authors proposed a formulation to evaluate the shear strength of CRM-reinforced panels based on diagonal compression tests. From the formulation, the equivalent tensile strength of CRM-reinforced masonry can be calculated (see also [39]):

$$\tau_{0,R} = \beta(\tau_{0,URM} + \tau_{0,pl}\frac{t_{pl}}{t_m}). \quad (4)$$

Where $\tau_{0,pl} = f_{t,pl}/1.5$ is the shear strength of the plaster, t_{pl} is the overall thickness of the coating and β is a corrective coefficient obtained experimentally and varying between 0.80 and 1.20 for solid brick masonry. In the present work, the shear strength of the reinforced samples was calculated using Eq. (4) and assuming $\beta = 1.00$. the tensile strength of the plaster obtained from clamping grip tests was used, namely $f_{t,pl}$ = 0.90 MPa. Concerning the flexural capacity, the strength was calculated considering the composite masonry-CRM cross-section with the following assumptions:

- Perfect adhesion between CRM and support. Any plane section remains plane.
- Masonry and mortar characterised by zero tensile strength.
- Masonry and mortar characterised by stress block constitutive law in compression, by assuming ε_0 = 0.07% and ε_u= 0.35% for both of them and f_{cm}= 14.40 MPa and $f_{c,pl}$= 13.80 MPa.
- GFRP grid characterised by linear elastic brittle behaviour. The ultimate stress, strain and elastic modulus were the ones experimentally obtained from tensile tests on twisted yarns, arranged in Y direction, namely f_y = 641 MPa, ε_y = 1.84%, and E_y = 35,100 MPa.
- Failure reached due to masonry and mortar crushing (ε_m=ε_{pl}=ε_u=0.35%) or due to GFRP grid tensile rupture (ε_f=ε_y =1.84%).

Table 8
Comparison between experimental and analytical flexural and shear strength of unreinforced and reinforced walls. The differences Δ are calculated referring to the failure mechanism experimentally obtained.

	FM	V_{max_exp} [kN]	$V_{max,flex}$ [kN]	$V_{max,shear}$ [kN]	Δ [%]
SC_URM_01	Flexural	176	172	179	-2%
SC_URM_02	Flexural	173			-1%
SC_RM_2_01	Shear	198	237	249	26%
SC_RM_2_02	Shear	214			16%
SC_RM_1_01	Shear	188	206	215	14%
SC_RM_1_02	Flexural	204			1%

In Table 8 the resistances obtained experimentally have been compared with the values obtained using the analytical procedures.

The comparison of the results shows that the analytical model estimated well the flexural strength of the unreinforced panels, demonstrating the reliability of the setup. Furthermore, the strength $V_{max,shear}$ of unreinforced wall calculated with the estimated value of τ_0 resulted only slightly greater than the flexural strength. This result is consistent with the experiments: considering the failure of the specimen *SC_URM_01*, in which the opening of a wide diagonal crack occurred after several cycles of rocking (see Fig. 16 b), a shear strength close to the flexural one was to be expected. Focusing on reinforced walls, the numerical formulation (4) used to compute the shear strength overestimated the experimental values. The comparison between numerical and experimental results of the specimens that exhibited a shear failure provided the largest differences, + 26% and + 16% for panels reinforced on two sides belonging to set 1 and 2, respectively, and + 14% for the panel asymmetrically strengthened. These differences can be attributed to the detachment of the coating layers observed during shear tests, which limited the efficiency of the CRM. Indeed, Eq. (4) was developed under the assumption of perfect adhesion with the support. The difference is more pronounced in the first set of tests, where the punctual application of the load favoured the detachment. This comparison suggests that the correction coefficient β should be calibrated to account for possible debonding. Equalising the experimental values to analytical ones at varying β, the following values of the correction coefficient have been obtained: 0.69, 0.80 and 0.80 for *SC_RM_2_01, SC_RM_2_02* and *SC_RM_1_01*, respectively. It is worth noting that the values obtained fall within the range of variability proposed by the authors in [38], except to the first related to the test of the first set in which the detachment was favoured by the load application. Finally, the single-sided reinforced specimen *SC_CRM_1_02* showed a flexural failure: the calculation of the flexural strength of the CRM-reinforced composed cross-section predicted the experimental capacity with good accuracy (+1%).

6. Conclusions

This work presented the main results of an experimental campaign carried out to study the efficiency of a CRM system in improving the compression and lateral response of brick masonry panels. Characterisation tests were performed to assess the mechanical properties of CRM components and their interaction with the substrate. Tensile tests on CRM coupons showed the trilinear behaviour of the composite and provided the slip resistance at the fibre-matrix interface and the tensile strength and Young modulus of the mortar. Shear bond tests pointed out

that the weakest mechanism of the system was the debonding of the coating from the support, and an average value of the interface resistance $\tau_u = 0.24$ MPa was obtained. Then, compression and shear-compression tests were carried out to investigate the response of strengthened walls. Two concentric and one eccentric compression tests have been performed to evaluate the CRM efficiency in increasing the load-bearing capacity of masonry columns. Results of centred compression tests have shown a low effect of the CRM due to the detachment between the coating and the support, favoured by the absence of transversal connectors not applied in the compression tests. Further experimental investigations should be carried out to assess the influence of connectors on the load-bearing capacity of CRM-reinforced panels. The contribution of the coating appeared to be greater in the case of eccentric application of the load, thanks to the tensile strength of the system which postponed the out-of-plane buckling. Samples centred loaded showed a quite similar load-bearing capacity, regardless of the application of the CRM system on one or two sides of the wall, namely $P_{u,1side} = 287$ kN and $P_{u,2sides} = 296$ kN, respectively. The sample subjected to eccentric compression showed an ultimate load, $P_u = 191$ kN, lower than the previous ones due to the bending induced by the eccentricity. The results pointed out the positive contribution of the CRM in limiting the out-of-plane deflection of slender walls. Six shear-compression tests were carried out using a cantilever static scheme equipped with middle-height support to investigate the influence of the grid anchoring on the flexural behaviour of walls. Two sets of tests were performed depending on the modality of application of the vertical and horizontal loads at the top of the walls. Amplification coefficients of strength, stiffness and ultimate displacement were defined to quantify the contribution of the CRM; moreover, the cumulative energy dissipated by the hysteretic cycles was calculated. An amplification of 13% and 7% in strength has been obtained for the two-sided and the one-sided strengthened panels belonging to the first set of tests, while an amplification of 24% and 18% in strength has been obtained for the corresponding panels of the second set. Conversely, the application of the reinforcement has led to a slight reduction of the displacement capacity of the panels due to the contrast offered by the CRM layers to the free rocking, changing the failure mechanism from a flexural to a shear rupture. A reduction of 13% (two layers of CRM) and 28% (one layer of CRM) was obtained for the panels belonging to the first set, and a reduction of 20% (two layers) and 12% (one layer) was obtained for the panels of the second set. Nevertheless, the cumulative dissipated energy at the end of the cyclic response was computed for all the specimens, evidencing that the presence of the reinforcement system led to a significant increase in dissipation; in particular, an increase in the capacity to dissipate energy of 71% and 35% when strengthened on one side and of 152% and 93% when strengthened on two sides was obtained. In reinforced walls, the detachment of the coating layers from the masonry was observed once the first wide cracks appeared, starting from the corners, where the compressive stresses show their peak values. After the detachment, the presence of steel connectors ensured the integrity of the panel despite the significant damage. Finally, a comparison between the flexural and shear strength obtained in the experimental tests and some analytical models proposed in the literature was made to evaluate the reliability of the results. The models for assessing the flexural strength showed a good agreement with experimental values, while the analytical procedures for estimating the shear strength of strengthened panels overestimated the experimental results due to the premature detachment between the support and plaster. The results of this study will be used in future works for the calibration of a numerical model capable of reproducing the static and seismic response of reinforced and unreinforced panels, necessary to extend the experimental results herein described and to deeply investigate the behaviour of CRM-strengthened masonry.

CRediT authorship contribution statement

Vienni Carlo: Conceptualization, Data curation, Writing – original draft, Writing – review & editing, Formal analysis, Investigation, Visualization. **Orlando Maurizio:** Conceptualization, Funding acquisition, Project administration, Supervision, Writing – review & editing, Resources, Investigation. **Salvatori Luca:** Conceptualization, Funding acquisition, Supervision, Writing – review & editing, Project administration, Resources, Investigation.

Declaration of Competing Interest

The authors declare that they have no known competing financial interests or personal relationships that could have appeared to influence the work reported in this paper.

Data availability

Data will be made available on request.

References

[1] CNR-DT-200, "Istruzioni per la progettazione, l'esecuzione ed il controllo di interventi di consolidamento statico mediante l'utilizzo di compositi fibrorinforzati (in Italian), Consiglio Nazionale delle Ricerche," 2013.

[2] CNR-DT-215, "Istruzioni per la Progettazione, l'Esecuzione ed il Controllo di Interventi di Consolidamento Statico mediante l'utilizzo di Compositi Fibrorinforzati a Matrice Inorganica." 2018.

[3] Papanicolaou CG, Triantafillou TC, Karlos K, Papathanasiou M. Textile-reinforced mortar (TRM) versus FRP as strengthening material of URM walls: In-plane cyclic loading. Mater Struct/Mater Constr 2007;40(10):1081–97. https://doi.org/10.1617/s11527-006-9207-8.

[4] Gioffrè M, Cavalagli N, Gusella V, Pepi C. Confined vs. unreinforced masonry: construction and shaking table tests of two-storey buildings. Constr Build Mater 2022;333. https://doi.org/10.1016/j.conbuildmat.2022.126961.

[5] Gattesco N, Rizzi E, Facconi L, Minelli F, Dudine A. Investigating the effectiveness of a CRM system: full scale reverse cyclic tests on a two-storey rubblestone masonry building. Procedia Struct Integr 2023;44:2222–9. https://doi.org/10.1016/j.prostr.2023.01.284.

[6] D'Antino T, Calabrese AS, Poggi C. Experimental procedures for the mechanical characterization of composite reinforced mortar (CRM) systems for retrofitting of masonry structures. Mater Struct/Mater Constr 2020;53(4):1–18. https://doi.org/10.1617/s11527-020-01529-1.

[7] Gattesco N, Boem I. Characterization tests of GFRM coating as a strengthening technique for masonry buildings. Compos Struct 2017;165:209–22. https://doi.org/10.1016/j.compstruct.2017.01.043.

[8] Borri A, Corradi M, Sisti R, Buratti C, Belloni E, Moretti E. Masonry wall panels retrofitted with thermal-insulating GFRP-reinforced jacketing. Mater Struct/Mater Constr 2016;49(10):3957–68. https://doi.org/10.1617/s11527-015-0766-4.

[9] Angiolilli M, Gregori A, Cattari S. Performance of fiber reinforced mortar coating for irregular stone masonry: experimental and analytical investigations. Constr Build Mater 2021;294:123508. https://doi.org/10.1016/j.conbuildmat.2021.123508.

[10] del Zoppo M, di Ludovico M, Balsamo A, Prota A. In-plane shear capacity of tuff masonry walls with traditional and innovative composite reinforced mortars (CRM). Constr Build Mater 2019;210:289–300. https://doi.org/10.1016/j.conbuildmat.2019.03.133.

[11] Cavalagli N, Gioffrè M, Gusella V, Pepi C, Baietti B, Mantegazza G, et al. In situ shear tests on masonry panels strengthened with fiber-reinforced mortar repointing. Key Engineering Materials. Trans Tech Publications Ltd,; 2017. p. 282–8. doi: 10.4028/www.scientific.net/KEM.747.282.

[12] Borri A, Castori G, Corradi M. Design criteria for masonry reinforcement with composite reinforced mortars (CRM). Key Eng Mater 2022;(December):498–504. https://doi.org/10.4028/p-k031gd.

[13] Boem I. Masonry elements strengthened with TRM: a review of experimental, design and numerical methods. Buildings 2022;2022(12):1307. https://doi.org/10.3390/buildings12091307.

[14] Gattesco N, Rizzi E, Bez A, Dudine A. Study on the effectiveness of a CRM system: in-plane and out-of-plane cyclic tests on masonry piers. Procedia Struct Integr 2023;44:2230–7. https://doi.org/10.1016/j.prostr.2023.01.285.

[15] Guerrini G, Bruggi A, Urso S, Quaini M, Penna A. Cyclic shear-compression tests on two stone masonry piers strengthened with CRM and FRCM. Procedia Struct Integr 2023;44:2214–21. https://doi.org/10.1016/j.prostr.2023.01.283.

[16] CSLLPP-n.7, "Circolare 21 gennaio 2019 n.7 Istruzioni per l'applicazione dell'"Aggiornamento delle 'Norme tecniche per le costruzioni'" di cui al decreto ministeriale 17 gennaio 2018. (Italian Guideline)," Supplemento ordinario alla

"Gazzetta Ufficiale., n. 35 del 11 febbraio 2019 - Serie generale, p. 337, 2019, [Online]. Available: ⟨https://www.gazzettaufficiale.it/eli/gu/2019/02/11/35/so/5/sg/pdf⟩.
[17] M. NTC 2018, "Aggiornamento delle 'Norme tecniche per le costruzioni' NTC 2018," pp. 1–198, 2018.
[18] Donnini J, Maracchini G, Lenci S, Corinaldesi V, Quagliarini E. TRM reinforced tuff and fired clay brick masonry: Experimental and analytical investigation on their in-plane and out-of-plane behavior. Constr Build Mater 2021;272:121643. https://doi.org/10.1016/j.conbuildmat.2020.121643.
[19] Pinho FFS, Lúcio VJG, Baião MFC. Rubble stone masonry walls in Portugal strengthened with reinforced micro-concrete layers. Bull Earthq Eng 2012;10(1):161–80. https://doi.org/10.1007/s10518-011-9280-4.
[20] Bernat E, Gil L, Roca P, Escrig C. Experimental and analytical study of TRM strengthened brickwork walls under eccentric compressive loading. Constr Build Mater 2013;44:35–47. https://doi.org/10.1016/j.conbuildmat.2013.03.006.
[21] Vienni C, Salvatori L, Orlando M. Cyclic shear-compression tests on CRM reinforced brick masonry walls. Procedia Struct Integr 2023;44:2262–9. https://doi.org/10.1016/j.prostr.2023.01.289.
[22] Vienni C, Orlando M, Salvatori L. CRM reinforced brick masonry walls: experimental and parametric numerical investigations. Procedia Struct Integr 2023;vol. 44:2270–7. https://doi.org/10.1016/j.prostr.2023.01.290.
[23] EN 772–1, "Metodi di prova per muratura," vol. 4, 2002.
[24] UNI_EN_1015–11, "Metodi di prova per malte per opere murarie Parte 11: Determinazione della resistenza a flessione e a compressione della malta indurita UNI EN 1015–11," no. 5972936, 2007.
[25] UNI-EN-1052–1, "Methods of tests for masonry. Determination of compressive strength," vol. 4, 2001.
[26] Ruregold, Eta 22–0078 PROPRIETA ' DELLA RETE PREFORMATA IN FRP – INTONACO ARMATO CRM Allegato A1," (in Italian) p. 2022, 2022.
[27] CSLLPP, "Linea Guida per la identificazione, la qualificazione ed il controllo di accettazione dei sistemi a rete preformata in materiali compositi fibrorinforzati a matrice polimerica da utilizzarsi per il consolidamento strutturale di costruzioni esistenti con l," pp. 1–38, 2019.
[28] CSLLPP, "Linee guida per la identificazione, la qualificazione edil controllo di accettazione di compositi fibrorinforzati a matrice inorganica (FRCM)," Cemento, vol. 93, pp. 62–00146, 2018.
[29] AC434, "Acceptance criteria for concrete and masonry strengthening using fabric-reinforced cementitious matrix (FRCM) composite Systems," ICC Evaluation Service, Whittier, CA, no. 2018.
[30] de Santis S, de Felice G. Tensile behaviour of mortar-based composites for externally bonded reinforcement systems. " *Compos B Eng* 2015;vol. 68:401–13. https://doi.org/10.1016/j.compositesb.2014.09.011.
[31] CEB-FIP, Model Code 90. 1990.
[32] "Calvi_Magenes 1996_Testing Masonry structures.pdf."
[33] Morandi P, Albanesi L, Graziotti F, Li Piani T, Penna A, Magenes G. Development of a dataset on the in-plane experimental response of URM piers with bricks and blocks. Constr Build Mater 2018;190:593–611. https://doi.org/10.1016/j.conbuildmat.2018.09.070.
[34] Magenes G, Calvi GM. In-plane seismic response of brick masonry walls. Earthq Eng Struct Dyn 1997;26(11):1091–112. https://doi.org/10.1002/(SICI)1096-9845(199711)26:11<1091::AID-EQE693>3.0.CO;2-6.
[35] Vanin F, Zaganelli D, Penna A, Beyer K. Estimates for the stiffness, strength and drift capacity of stone masonry walls based on 123 quasi-static cyclic tests reported in the literature. Bull Earthq Eng 2017;15(12):5435–79. https://doi.org/10.1007/s10518-017-0188-5.
[36] Godio M, Vanin F, Zhang S, Beyer K. Quasi-static shear-compression tests on stone masonry walls with plaster: influence of load history and axial load ratio. Eng Struct 2019;192(April):264–78. https://doi.org/10.1016/j.engstruct.2019.04.041.
[37] D'Antino T, Carozzi FG, Poggi C. Diagonal shear behavior of historic walls strengthened with composite reinforced mortar (CRM). Mater Struct/Mater Constr 2019;52(6):1–15. https://doi.org/10.1617/s11527-019-1414-1.
[38] Gattesco N, Boem I. Experimental and analytical study to evaluate the effectiveness of an in-plane reinforcement for masonry walls using GFRP meshes. Constr Build Mater 2015;88:94–104. https://doi.org/10.1016/j.conbuildmat.2015.04.014.
[39] I. Boem and N. Gattesco, Rehabilitation of masonry buildings with Fibre Reinforced Mortar: practical design considerations concerning seismic resistance, 2021.